



Intense molybdenum accumulation in sediments underneath a nitrogenous water column and implications for the reconstruction of paleo-redox conditions based on molybdenum isotopes

Florian Scholz^{*}, Christopher Siebert, Andrew W. Dale, Martin Frank

GEOMAR Helmholtz Centre for Ocean Research Kiel, Wischhofstraße 1-3, 24148 Kiel, Germany

Received 26 January 2017; accepted in revised form 29 June 2017; Available online 11 July 2017

Abstract

The concentration and isotope composition of molybdenum (Mo) in sediments and sedimentary rocks are widely used proxies for anoxic conditions in the water column of paleo-marine systems. While the mechanisms leading to Mo fixation in modern restricted basins with anoxic and sulfidic (euxinic) conditions are reasonably well constrained, few studies have focused on Mo cycling in the context of open-marine anoxia. Here we present Mo data for water column particulate matter, modern surface sediments and a paleo-record covering the last 140,000 years from the Peruvian continental margin. Mo concentrations in late Holocene and Eemian (penultimate interglacial) shelf sediments off Peru range from ~ 70 to $100 \mu\text{g g}^{-1}$, an extent of Mo enrichment that is thought to be indicative of (and limited to) euxinic systems. To investigate if this putative anomaly could be related to the occasional occurrence of sulfidic conditions in the water column overlying the Peruvian shelf, we compared trace metal (Mo, vanadium, uranium) enrichments in particulate matter from oxic, nitrate-reducing (nitrogenous) and sulfidic water masses. Coincident enrichments of iron (Fe) (oxyhydr)oxides and Mo in the nitrogenous water column as well as co-variation of dissolved Fe and Mo in the sediment pore water suggest that Mo is delivered to the sediment surface by Fe (oxyhydr)oxides. Most of these precipitate in the anoxic-nitrogenous water column due to oxidation of sediment-derived dissolved Fe with nitrate as a terminal electron acceptor. Upon reductive dissolution in the surface sediment, a fraction of the Fe and Mo is re-precipitated through interaction with pore water sulfide. The Fe- and nitrate-dependent mechanism of Mo accumulation proposed here is supported by the sedimentary Mo isotope composition, which is consistent with Mo adsorption onto Fe (oxyhydr)oxides. Trace metal co-variation patterns as well as Mo and nitrogen isotope systematics suggest that the same mechanism of Mo delivery caused the ‘anomalously’ high interglacial Mo accumulation rates in the paleo-record. Our findings suggest that Fe- and nitrate-dependent Mo shuttling under nitrogenous conditions needs to be considered a possible reason for sedimentary Mo enrichments during past periods of widespread anoxia in the open ocean.

© 2017 Elsevier Ltd. All rights reserved.

Keywords: Paleo-redox; Molybdenum isotopes; Early diagenesis; Oxygen minimum zone; Anoxic marine sediment

1. INTRODUCTION

1.1. Scientific rationale

The Peruvian continental margin and associated oxygen minimum zone (OMZ) represent one of the most extreme

^{*} Corresponding author.

E-mail address: fscholz@geomar.de (F. Scholz).

open-marine redox environments in the contemporary ocean. Oxygen concentrations in the core of the Peruvian OMZ (~100–300 m water depth, 10–20 °S) remain below the detection limit of state-of-the-art micro-sensors most of the time (<10 nM O₂) (Thamdrup et al., 2012). Moreover, stagnation events, during which hydrogen sulfide (H₂S) is released from the sediment into the water column, have been reported in recent studies (Schunck et al., 2013; Sommer et al., 2016). As a consequence of these unique characteristics, the Peruvian margin is an excellent locality to calibrate paleo-redox proxies in the context of open-marine anoxia.

It could be argued that restricted anoxic basins such as the Black Sea and Baltic Sea Deeps represent more appropriate analogues for extreme anoxia in Earth history than upwelling regions like the Peruvian margin. This notion is largely based on chemical arguments such as the more persistent occurrence of sulfidic conditions and higher H₂S concentrations in the water column of these systems compared to modern open ocean settings (Richards, 1965). However, the enclosed bathymetry, restricted estuarine circulation pattern and long seawater residence time in silled basins limit the comparability to open-marine systems in the geological past (e.g., Emerson and Husted, 1991; Algeo and Lyons, 2006; Scholz et al., 2013, 2014a). This is particularly true for paleo-systems characterized by complex lateral and vertical redox-structures, as suggested for several key periods and events in Earth history (e.g., Poulton et al., 2010; Hammarlund et al., 2012; Westermann et al., 2014; Goldberg et al., 2016), rather than uniform and basin-wide anoxia.

Here, we investigate the behavior of molybdenum (Mo) in the water column and sediments of the Peruvian continental margin. The main purpose of this study is to gain a mechanistic understanding of the factors controlling the concentration and isotope composition of Mo in sediments that accumulate in an open-marine anoxic environment. We also evaluate the likelihood that similar mechanisms operated during past periods of widespread anoxia in the open ocean.

1.2. The molybdenum proxy

Sedimentary Mo concentrations and isotope compositions are (along with iron (Fe) speciation) the most commonly used proxies for the identification of anoxic and sulfidic (i.e., euxinic) conditions in the water column of ancient marine systems. Molybdenum has a long residence time (~440,000 years) (Miller et al., 2011) in oxygenated seawater and thus a uniform concentration (~110 nM at a salinity of 35) throughout the global ocean (Bruland, 1983). In the presence of dissolved H₂S, molybdate (MoO₄²⁻), the stable Mo species in oxygenated seawater, is converted to sulfur-containing Mo complexes (e.g., thiomolybdate (Mo^VO_xS_{4-x}²⁻, 1 < x < 4) or Mo polysulfide (Mo^{IV}O(S₄S²⁻)) (Helz et al., 1996; Erickson and Helz, 2000; Vorlicek et al., 2004; Dahl et al., 2013a). Thiomolybdate or Mo polysulfide (hereafter referred to as Mo-S species) are particle reactive and show a strong affinity to Fe sulfide minerals and sulfur-rich organic matter (Huerta-

Diaz and Morse, 1992; Zheng et al., 2000; Vorlicek and Helz, 2002; Vorlicek et al., 2004; Tribovillard et al., 2004; Helz et al., 2011). This leads to an efficient mechanism of Mo fixation under sulfidic conditions. Therefore, marine systems in which H₂S is present in the shallow sediment or bottom waters are typically characterized by sedimentary Mo enrichments. In general, the extent of Mo enrichment increases from environments where H₂S is only present in the sediment pore water to environments where H₂S accumulates in the water column. Based on this observation, previous studies have proposed that sedimentary Mo concentrations >25 µg g⁻¹ are indicative of at least intermittently euxinic conditions (Scott and Lyons, 2012; Dahl et al., 2013b). In some cases, sedimentary Mo enrichments in euxinic settings can be masked by dilution with detrital material (Scott and Lyons, 2012). Moreover, sustained periods of Mo fixation in euxinic basins with a long seawater residence time can lead to a drawdown of the Mo inventory in the water column (Algeo, 2004; Algeo and Lyons, 2006) thus impeding significant Mo enrichment (i.e., >>25 µg g⁻¹) in the sediment.

The relatively heavy Mo isotope composition of modern seawater (δ⁹⁸Mo = 2.3‰) has been attributed to the balance between the terrigenous input flux supplied via weathering and continental runoff (average δ⁹⁸Mo of +0.7‰) (Archer and Vance, 2008) and an isotopically light sink associated with Mo adsorption onto manganese (Mn) (oxy-

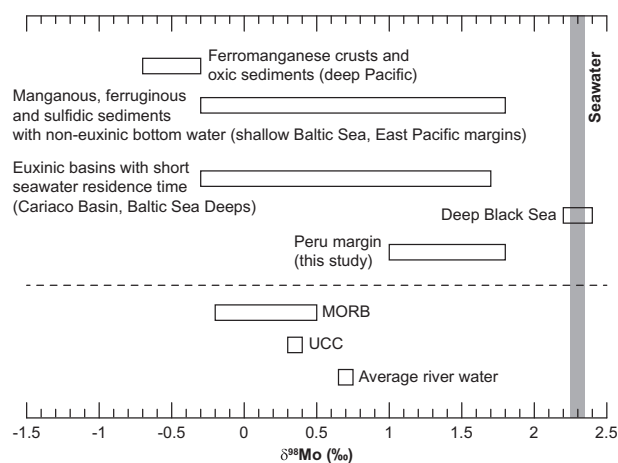


Fig. 1. Schematic overview of the range of Mo isotope values at different type localities in the contemporary ocean: Ferromanganese crusts and oxic sediments in the deep-sea (Barling et al., 2001; Poulson et al., 2006; Poulson Brucker et al., 2009); manganous, ferruginous and sulfidic sediments at continental margins (Poulson et al., 2006; Poulson Brucker et al., 2009; Goldberg et al., 2012); euxinic basins with a short seawater residence time (~≤100 years; Baltic Sea Deeps, Cariaco Basin) (Arnold et al., 2004; Noordmann et al., 2015); euxinic basin with a long seawater residence time (hundreds to thousands of years; Black Sea) (Barling et al., 2001; Arnold et al., 2004). The range of isotope values observed in the present study as well as the Mo isotope compositions of Mid-ocean ridge basalt (MORB) (Freymuth et al., 2015), upper continental crust (UCC) (Voegelin et al., 2014) and average river water (Archer and Vance, 2008) are shown for comparison.

hydr)oxides in oxic deep-sea sediments (Barling et al., 2001; Siebert et al., 2003) (Fig. 1). Early in the history of Mo isotope geochemical research, it was discovered that sediments in the euxinic Black Sea have a Mo isotope composition similar to oxic seawater (Barling et al., 2001; Arnold et al., 2004) (Fig. 1). Based on the assumption that sediments underneath euxinic waters generally record the Mo isotope composition of contemporary seawater, it was argued that if large parts of the ocean remained euxinic for a prolonged period of time (theoretically implying near-quantitative Mo removal with no apparent isotope fractionation) the isotope composition of seawater would reach a new steady state value that lies closer to the $\delta^{98}\text{Mo}$ of the Mo input flux from rivers. Following this concept, black shales with a $\delta^{98}\text{Mo}$ below contemporary seawater and Black Sea sediments (below the chemocline) combined with independent evidence for euxinic conditions (e.g., from Fe speciation) have been interpreted as a quantitative indicator for more expanded euxinia during the corresponding intervals in Earth history (e.g., Arnold et al., 2004; Wille et al., 2008; Kendall et al., 2009; Dahl et al., 2011; Goldberg et al., 2016).

It is important to note, however, that the Black Sea is the only large euxinic basin investigated to date where the sedimentary Mo isotope signature reflects the $\delta^{98}\text{Mo}$ of contemporary seawater. In all other large euxinic basins investigated so far, $\delta^{98}\text{Mo}$ values span the entire range between the isotopically light oxic sink and modern seawater (see Fig. 1 and compilation in Goldberg et al. (2016)) thus implying partial removal of a fractionated Mo pool. In fact, the sedimentary Mo isotope values reported for most euxinic settings are similar to those observed in settings where H_2S is only present in the sediment pore water (Fig. 1). Such sulfidic continental margin sediments represent another important sink in the global ocean's Mo mass balance (McManus et al., 2006; Poulson Brucker et al., 2009).

Essentially two different mechanisms have been invoked to explain the Mo isotopic offset between sediments and seawater in both euxinic and non-euxinic settings: The first explanation is related to an incomplete conversion of molybdate to thiomolybdate species followed by partial removal of the latter (Neubert et al., 2008; Dahl et al., 2010; Nägler et al., 2011). The change in aqueous Mo speciation is expected to be accompanied by isotope fractionation (Tossell, 2005) and should thus impart an isotopic offset in the solid phase if one of the species is preferentially removed. The conversion of molybdate to thiomolybdate is a function of the H_2S concentration (Helz et al., 1996), which is why incomplete conversion in many euxinic settings could be the result of lower H_2S concentrations than those prevailing in the Black Sea.

The second explanation is related to the deposition of a particulate phase where Mo is adsorbed to the surfaces of metal (oxyhydr)oxides (McManus et al., 2002; Poulson Brucker et al., 2009; Goldberg et al., 2012). Experimental studies have demonstrated that the light Mo isotopes preferentially adsorb to the surfaces of Mn and Fe (oxyhydr)oxide minerals. The extent of isotope fractionation decreases from Mn ($\Delta^{98}\text{Mo}_{\text{seawater-adsorbed}} = +2.8\%$)

(Siebert et al., 2003; Barling and Anbar, 2004; Wasylenki et al., 2008) to Fe minerals ($\Delta^{98}\text{Mo}_{\text{seawater-adsorbed}} = +0.8 - +2.2\%$) and with decreasing crystallinity of the Fe (oxyhydr)oxides: hematite ($\Delta^{98}\text{Mo}_{\text{seawater-adsorbed}} = +2.19 \pm 0.54\%$) > goethite ($\Delta^{98}\text{Mo}_{\text{seawater-adsorbed}} = +1.40 \pm 0.48\%$) > ferrihydrite ($\Delta^{98}\text{Mo}_{\text{seawater-adsorbed}} = +1.11 \pm 0.15\%$) (Goldberg et al., 2009). Release of Mo from Mn and/or Fe (oxyhydr)oxides followed by interaction with pore water sulfide and precipitation of an authigenic Mo phase would thus also produce a lighter Mo isotope value than seawater.

Even though the fundamental processes contributing to Mo isotope fractionation in marine sedimentary environments have been identified, the detailed pathway of Mo transfer from the water column into the sedimentary paleo-record is still poorly constrained. One reason for this knowledge gap is that, in most cases, either shallow sediments or paleo-records (mostly in deep time) are investigated but not both at the same site. Therefore, it is difficult to link the findings of regional process studies to paleo-signals and paleo-environmental conditions. Moreover, few Mo data for water column particulate matter are available. To overcome this situation, we present here Mo concentration data for water column particulate matter, shallow sediments and pore waters as well as a late Quaternary paleo-record. In addition, Mo isotope data for the shallow sediments and paleo-record are reported. All samples were taken in close proximity to each other on the Peruvian continental margin.

2. STUDY AREA AND SAMPLES

Wind-driven upwelling of nutrient-rich intermediate water off Peru results in high primary and export production. Due to low oxygen concentrations in the upwelling water masses and intense respiration of the downward sinking organic matter, the Peruvian upwelling system is characterized by a pronounced OMZ with essentially anoxic conditions between 100 and 300 m water depth (Fig. 2A) (Thamdrup et al., 2012). A permanent nitrate deficit and the presence of a secondary nitrite maximum in the oxygen minimum zone indicate that denitrification and anammox (anaerobic ammonium oxidation) are the dominant biogeochemical processes in the water column (Fig. 2B and C) (Lam et al., 2009; Dalsgaard et al., 2012). Denitrification, Fe reduction and bacterial sulfate reduction dominate organic matter respiration in the underlying surface sediments (Bohlen et al., 2011). Due to the absence of oxygen in the bottom water, dissolved ferrous Fe generated in the sediment diffuses across the sediment-water interface (Noffke et al., 2012) thus leading to elevated Fe concentrations in the water column (Bruland et al., 2005; Vedamati et al., 2014). A recent study using the same water column particulate matter samples as the present study has demonstrated that long distance transport of dissolved Fe in the anoxic water column is likely limited by Fe oxidation with nitrate as a terminal electron acceptor (Scholz et al., 2016).

Long-lasting periods of nitrate-reducing (i.e., nitrogenous) conditions in the water column are occasionally interrupted by oxygenation events, which are related to the

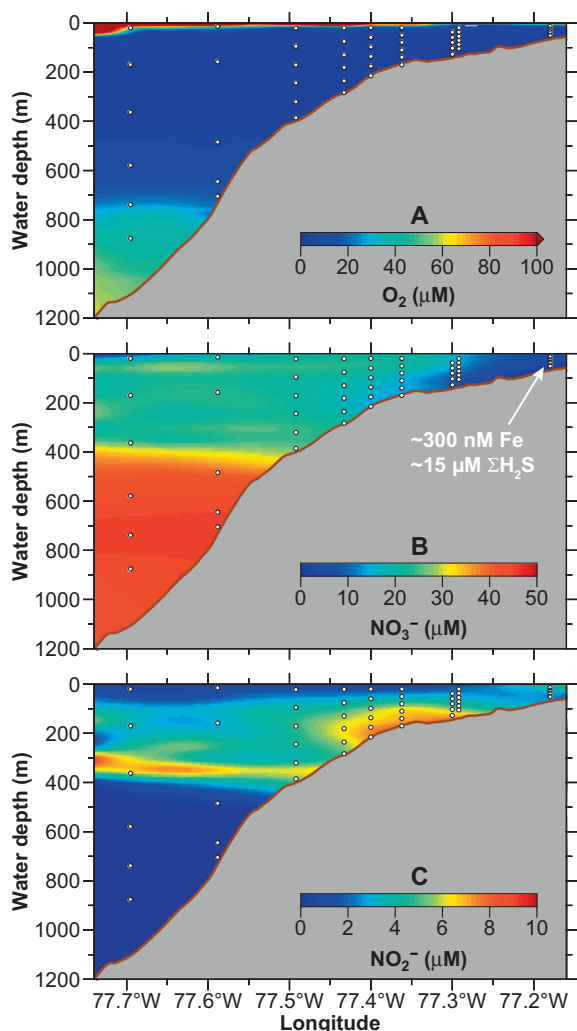


Fig. 2. Water column redox conditions across the Peruvian continental margin at 12°S (see Fig. 3 for location map) during research cruise M92 in January 2013 (data from Scholz et al., 2016): (A) O_2 , (B) nitrate (NO_3^-), (C) nitrite (NO_2^-). The nitrate- and nitrite-depleted water mass overlying the shelf was characterized by elevated dissolved Fe and H_2S concentrations (see arrow in (B)). Circles depict the location of particulate matter samples that were taken during the cruise.

passage of coastal trapped waves (Gutiérrez et al., 2008). Such transient oxygenation is most intense during El Niño events (e.g., $>20 \mu M O_2$ in bottom waters below 200 m water depth) (Levin et al., 2002). Sulfidic events, the opposite redox extreme in the water column overlying the Peruvian shelf, occur during times of water column stagnation. Upon complete consumption of nitrate and nitrite in the bottom water, H_2S is released from the sediment into the water column (Schunck et al., 2013; Dale et al., 2016). Pale-oceanographic studies have demonstrated that the OMZ off Peru and Chile was better ventilated during the last glacial maximum. By contrast, interglacials (Holocene and Eemian (MIS5e)) were characterized by more reducing conditions with more intense denitrification (Ganeshram et al., 2000; Muratli et al., 2010; Scholz et al., 2014b; Salvatelli et al., 2015).

Samples for this study were collected during three cruises of research vessel Meteor in November and December 2008 (cruises M77-1 and M77-2) and in January 2013 (M92) (Table 1). Water column particulate matter samples were collected during cruise M92 along a zonal section at 12°S (Fig. 3). During M92, the water column overlying the shallow shelf was characterized by weakly sulfidic conditions ($\Sigma H_2S = H_2S + HS^- + S^{2-} \sim 15 \mu M$) and high dissolved Fe concentrations (dissolved Fe = $\sim 300 nM$) (Fig. 2B) (Scholz et al., 2016). Shallow sediment cores were collected on a transect at 11°S during cruises M77-1 and M77-2 (Fig. 3). No hydrogen sulfide was detected in the water column during these cruises. The piston core from which the paleo-record investigated in this study was derived (piston core M77-2-024-5) was retrieved at $\sim 11^\circ$ at 210 m water depth, i.e., close to the shorter sediment cores MUC29 and BIGO-T (Table 1, Fig. 3). The age model of M77-2-024-5 was established by a combination of radiocarbon dating on organic matter and stratigraphic correlation with other records (see Scholz et al., 2014b for details). With the exception of a hiatus at 423 cm core depth ($\sim 50,000$ – $20,000$ yr BP), the age model of M77-2-024-5 covers the last 140,000 yrs. Some of the data used in this article were published previously (trace metal concentrations in sediments (Scholz et al., 2011, 2014b), pore water concentration data (Scholz et al., 2011), Fe speciation data (Scholz et al., 2014c)). All Mo isotope data as well as the trace metal concentration data for suspended particulate matter samples are new to this study.

3. METHODS

3.1. Sampling

Water column particulate matter samples were collected using an array of six PTFE-coated 8 L GO-FLO bottles (General Oceanics) individually mounted on a Kevlar wire. Upon recovery, the GO-FLO bottles were transferred to a laboratory and pressurized with nitrogen gas. The water was filtered through polyethersulfone filters (0.2 μm pore size, 47 mm) (PALL Corporation) in a laminar flow bench. Prior to use the filters had been leached with 1 M HCl and rinsed with deionized water. The filters were transferred to acid-cleaned Petri dishes and stored at $-20^\circ C$ until further treatment after the cruise. Shallow sediments (uppermost 15–30 cm) were collected using a multiple corer (MUC) or benthic landers (Biogeochemical Observatory, BIGO). Subsampling of the sediment cores was done in an argon-filled glove bag as described in detail in Scholz et al. (2011). The pore water was separated from the solid phase by centrifuging and filtered in a second glove bag through cellulose acetate membrane filters (0.2 μm pore size). The pore water aliquots for trace metal analyses were acidified using concentrated HNO_3 (purified by sub-boiling distillation) and stored in acid-cleaned HDPE vials. The residual sediment in centrifuge tubes was frozen and stored for solid phase analyses after the cruise. Sediment core M77-2-024-5 was retrieved with a piston corer and sediment samples were collected with cut syringes at the GEOMAR core repository.

Table 1
Geographical coordinates and water depth of all sampling stations.

Cruise	Station	Code	Longitude W	Latitude S	Water depth (m)	Bottom water oxygen ^{a, b} (μM)
<i>Water column</i>						
M92	72	GO-FLO05	12°13.5'	77°10.8'	74	
M92	212	GO-FLO11	12°18.9'	77°17.5'	144	
M92	60	GO-FLO04	12°18.7'	77°18.0'	145	
M92	278	GO-FLO12	12°21.5'	77°21.7'	195	
M92	31	GO-FLO03	12°23.0'	77°24.0'	244	
M92	112	GO-FLO07	12°24.8'	77°26.0'	298	
M92	135	GO-FLO09	12°27.2'	77°29.5'	407	
M92	102	GO-FLO06	12°31.3'	77°35.3'	774	
M92	126	GO-FLO08	12°35.9'	77°41.7'	1022	
<i>Sediment cores</i>						
M77-1	568	BIGO05	11°00.0'	77°47.7'	85	<LD
M77-1	470	MUC29	11°00.0'	77°56.6'	145	<LD
M77-2	016	BIGO-T	10°59.8'	78°05.9'	259	<LD
M77-1	449	MUC19	11°00.0'	78°10.0'	319	<LD
M77-1	459	MUC25	11°00.0'	78°25.6'	697	12.1
<i>Paleo-record</i>						
M77-2		M77-2-024-5	11°05.0'	78°00.91'	210	

LD: Limit of detection.

^a Shallow sediment cores only.

^b Bottom waters on the Peruvian shelf can be oxic or sulfidic (Scholz et al., 2011, 2016).

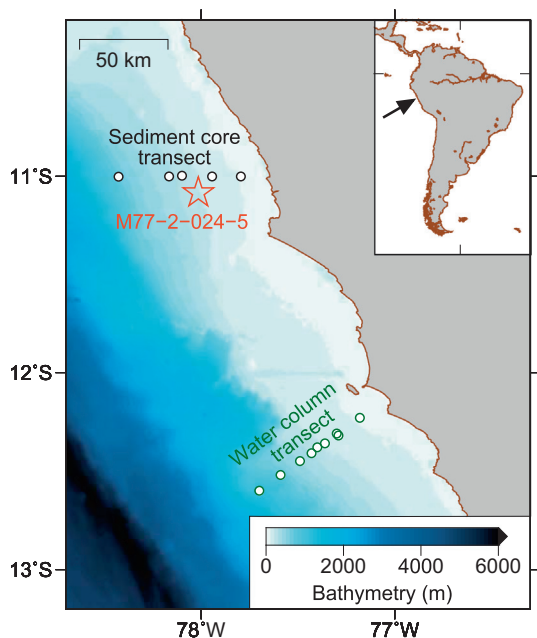


Fig. 3. Bathymetric map of the Peruvian continental margin showing the location of all GO-FLO (water column particulate matter) and sediment core stations.

3.2. Chemical analyses

Suspended particulate matter on filters was digested following the sampling and sample-handling protocols for GEOTRACES cruises (Cutter et al., 2014). In brief, filters

were cut into halves, placed into PTFE vials and the particles were digested through refluxing of HNO_3 and HF on a hot plate. After repeated evaporation of the solution and re-dissolution with concentrated HNO_3 , the residue was re-dissolved in 5 M HNO_3 and stored for further analysis. Sediment samples from MUCs and BIGOs were digested on a hotplate with an acid mix consisting of HNO_3 , HF and HClO_4 . Sediment samples from M77-2-024-5 were digested with a CEM MARS-5 microwave system in an acid mix consisting of HCl , HNO_3 and HF (Muratli et al., 2012). Major element (Fe, aluminum (Al), Mn) concentrations were analyzed by inductively coupled plasma optical emission spectrometry (ICP-OES) and trace element (vanadium (V), Mo, uranium (U)) concentrations were analyzed by inductively coupled plasma mass spectrometry (ICP-MS) (see Scholz et al. (2011, 2014b, 2016) for details). For quality control, blanks, sample duplicates and the certified reference materials SDO-1 (Devonian Ohio Shale, USGS) and MESS-3 (Marine Sediment, Canadian Research Council) as well as several in-house standards were included in the whole digestion and analysis procedure. Measured concentrations for certified reference materials were always within the certified ranges, except for Mo in MESS-3 following the digestion protocol for suspended particulate matter where the recovery was consistently about 20% too low. The digestion procedure for particulate matter is relatively gentle compared to the more aggressive protocols for sediment samples (lower acid concentrations and shorter digestion period) and residual sediment grains, presumably representing refractory minerals, were present after the digestion of MESS-3. Therefore, we attribute the incomplete recovery to the relatively low and crustal-like

Mo concentration in MESS-3 ($2.78 \pm 0.07 \mu\text{g g}^{-1}$; 2-fold enrichment over average upper continental crust). By contrast, particulate matter from the Peruvian margin is strongly enriched in Mo compared to crustal material (10^1 – 10^4 -fold enrichment over average upper continental crust) and suspended particulate matter samples did not reveal residual material after the digestion. We therefore consider the Mo concentrations obtained for particulate matter samples as reliable and unaffected by the incomplete recovery for MESS-3. Dissolved concentrations of Mo in pore water were also analyzed by ICP-MS. The accuracy and precision of these analyses was monitored by repeatedly analyzing certified reference material CASS-5 (Nearshore Seawater, Canadian Research Council) (recommended value: 102 nM; measured value (mean \pm standard deviation, SD): 95.4 ± 1.5 , $n = 87$).

To separate the authigenic from the lithogenic Mo fraction in the solid phase, trace metal concentrations are expressed as excess concentrations (Eq. (1)) or enrichment factors (Eq. (2)) relative to the trace metal (TM) to Al ratio of the regional lithogenic background (Brumsack, 2006; Tribouillard et al., 2006):

$$TM_{XS} = TM_{sample} - \frac{TM_{background}}{Al_{background}} \cdot Al_{sample} \quad (1)$$

$$TM_{EF} = \frac{\left(\frac{TM_{sample}}{Al_{sample}}\right)}{\left(\frac{TM_{background}}{Al_{background}}\right)} \quad (2)$$

Andesite in the Andean Arc was chosen as the regional lithogenic background ($\text{Fe}/\text{Al} = 0.47$, $\text{Mn}/\text{Al} = 1.23 \cdot 10^{-2}$, $\text{V}/\text{Al} = 1.39 \cdot 10^{-3}$, $\text{Mo}/\text{Al} = 0.26 \cdot 10^{-4}$, $\text{U}/\text{Al} = 0.37 \cdot 10^{-4}$) (Böning et al., 2004; Scholz et al., 2011).

3.3. Isotope analyses

Analysis of Mo isotopes in this study was performed at GEOMAR on a Nu Instruments multi collector ICP-MS with a DSN-100 Desolvation Nebulizer System utilizing a double isotope tracer (^{100}Mo , ^{97}Mo) for correction of instrumental and possible laboratory mass fractionation (Siebert et al., 2001). All samples were spiked with the tracer before chemical separation of Mo from the sample matrix. Chemical separation was performed in 0.5 M HCl on 2 mL of Biorad AG50W-X8 cation resin to remove Fe, followed by separation from the remaining matrix in 4 M HCl on 1 mL Biorad AG1-X8 anion exchange resin and elution in 2 M HNO_3 . Total procedural blanks were <1 ng of Mo.

During measurements 50 ng of Mo was analyzed resulting in an ion beam intensity of approximately 120 V ppm^{-1} (excluding double spike signal) using $10^{11} \Omega$ resistors. Each measurement is the average of 4 blocks of 10 measurement cycles with 10 s signal integration time each. Mass 99 was monitored for possible isobaric interferences of ruthenium. Samples were scanned for Fe before measurements to exclude possible Fe-argide interferences.

All Mo isotopic variations are presented in delta notation as the deviation of the $^{98}\text{Mo}/^{95}\text{Mo}$ ratio in parts per thousand (‰) relative to a standard:

$$\delta^{98}\text{Mo} = \left(\frac{\left(\frac{^{98}\text{Mo}}{^{95}\text{Mo}}\right)_{sample}}{\left(\frac{^{98}\text{Mo}}{^{95}\text{Mo}}\right)_{standard}} - 1 \right) \cdot 1000 \quad (3)$$

Isotope values in this study are presented relative to Alfa Aesar Mo plasma standard solution, Specpure #38791 (lot no. 011895D). This standard is offset from international interlaboratory reference material NIST SRM 3134 by a $\delta^{98}\text{Mo}$ value of $-0.15 \pm 0.03\text{‰}$ (2 SD) (Greber et al., 2012; Nägler et al., 2014). Nägler et al. (2014) suggested open-ocean seawater with a homogenous $\delta^{98}\text{Mo}$ of $+2.34 \pm 0.10\text{‰}$ (relative to NIST SRM 3134) as a secondary reference standard for Mo isotope measurement. Repeated analysis of IAPSO seawater standard in this study yielded a $\delta^{98}\text{Mo}$ of $+2.25 \pm 0.09\text{‰}$ (2 SD; $n = 4$), which is within analytical uncertainty of the internationally agreed seawater reference value. For information purposes, Mo isotope data are given relative to both the in-house standard and NIST SRM 3134 in Supplementary Tables S2 and S4.

USGS rock standard reference material SDO-1 (black shale) was processed through column chemistry and measured with each sample run. The long-term external reproducibility of SDO-1 is 0.09‰ (2 SD, average $\delta^{98}\text{Mo}$ is $+0.99\text{‰}$). Therefore, a uniform analytical error of $\pm 0.1\text{‰}$ is plotted in the figures. With the exception of a few samples from sediment core M77-2-024-5 (see Supplementary Table S4) sample duplicates are generally within this error range. The long-term external reproducibility of the Specpure standard solution is 0.07‰ (2 SD).

Analogous to Eq. (1) and assuming two-component-mixing of crustal Mo and authigenic Mo phases (Mo_{XS}), the isotope composition of Mo_{XS} is calculated according to the following mass balance equation:

$$\delta^{98}\text{Mo}_{XS} = \frac{\left(\delta^{98}\text{Mo}_{sample} - \left(1 - \frac{\text{Mo}_{XS}}{\text{Mo}_{sample}}\right) \cdot \delta^{98}\text{Mo}_{crust}\right)}{\left(\frac{\text{Mo}_{XS}}{\text{Mo}_{sample}}\right)} \quad (4)$$

Published estimates for the Phanerozoic average upper continental crust range from $+0.3\text{‰}$ to $+0.4\text{‰}$ (e.g., Malinovsky et al., 2007; Voegelin et al., 2014). In agreement with this range and following Goldberg et al. (2012) we chose to adopt $+0.3\text{‰}$ for $\delta^{98}\text{Mo}_{crust}$. Lithogenic contributions to the sedimentary Mo isotope signal observed in this study are generally low (<1% within the OMZ to 36% below the OMZ) so that using slightly higher or lower $\delta^{98}\text{Mo}_{crust}$ values would not affect the data interpretation.

4. RESULTS

4.1. Water column

Particulate metal concentrations in the water column are presented as a function of water depth and redox state (Fig. 4). Oxidic samples are from the surface ocean and below the OMZ, nitrogenous samples were taken within the OMZ and sulfidic samples were taken at the shallowest station within the sulfidic plume overlying the shelf sediments (Fig. 2).

Enrichment factors of Mo in suspended particulate matter are reported together with enrichment factors of other

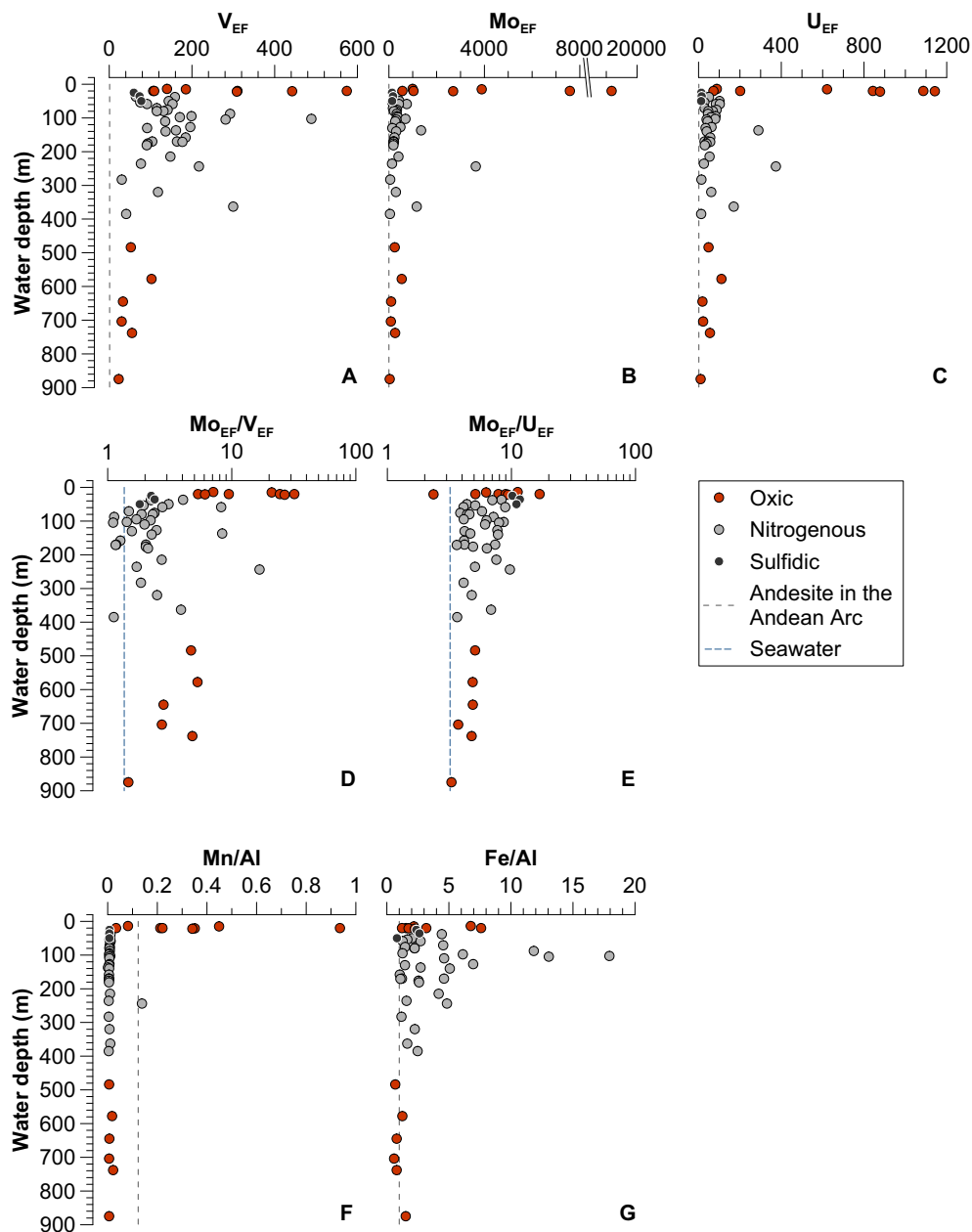


Fig. 4. Distribution of particulate metals in the water column: (A) V_{EF} , (B) Mo_{EF} , (C) U_{EF} , (D) Mo_{EF}/V_{EF} , (E) Mo_{EF}/U_{EF} , (F) Mn/Al, (G) Fe/Al). Samples are plotted against water depth and subdivided according to their redox state in oxic, nitrogenous and sulfidic. Vertical dashed lines depict the regional lithogenic background (andesite in the Andean Arc) or seawater (dissolved) Mo/V and Mo/U). The data shown in this figure are contained in [Supplementary Table S1](#).

metals that are known to be enriched in anoxic marine sediments. Trace metal enrichment factors decrease in the following order: oxic samples from the surface ocean > nitrogenous samples > sulfidic samples = oxic samples from below the OMZ (Fig. 4A–C). Enrichment factor ratios (Mo_{EF}/V_{EF} , Mo_{EF}/U_{EF}) are greater than one and exceed the seawater ratios in most samples (Fig. 4D and E). This observation indicates that Mo has the strongest affinity for suspended particulate matter among the trace metals investigated.

Particulate Mn and Fe concentrations are reported as Mn to Al and Fe to Al ratios which are compared to the Mn/Al and Fe/Al of the regional lithogenic background. In contrast to Mn and Fe, Al is not involved in redox-driven mineral dissolution or precipitation processes. Mn/Al and Fe/Al above or below the regional lithogenic background are thus indicative of in-situ precipitation or dissolution of Mn and Fe minerals. Suspended particulate matter in the well-oxygenated zone at the sea surface is enriched in Mn relative to the litho-

genic background (Fig. 4F). In contrast, sulfidic and nitrogenous samples as well as oxic samples from below the OMZ are Mn-depleted. Analogous to Mn, oxic samples from the surface ocean are enriched in Fe (Fig. 4G). However, nitrogenous samples from within the OMZ are characterized by even more pronounced Fe enrichments. Sulfidic samples and oxic samples from below the OMZ are characterized by Fe/Al similar to the lithogenic background.

4.2. Shallow sediment core transect

The highest Mo_{XS} concentrations ($\leq 100 \mu\text{g g}^{-1}$) are observed in sediments between ~ 100 and ~ 400 m water depth (Fig. 5A) where bottom waters are nitrogenous most of the time. Sediments on the shallow shelf (< 100 m water depth), where bottom waters can be oxic or sulfidic, and sediments below the OMZ (> 500 m water depth) are characterized by lower Mo_{XS} concentrations. Enrichment factor ratios ($\text{Mo}_{\text{EF}}/\text{V}_{\text{EF}}$, $\text{Mo}_{\text{EF}}/\text{U}_{\text{EF}}$) increase with decreasing water depth and reach the highest values at 145 m water depth (Fig. 5B and C) where they are broadly consistent with the enrichment factor ratios of particulate matter in the overlying water column (Fig. 4F and G).

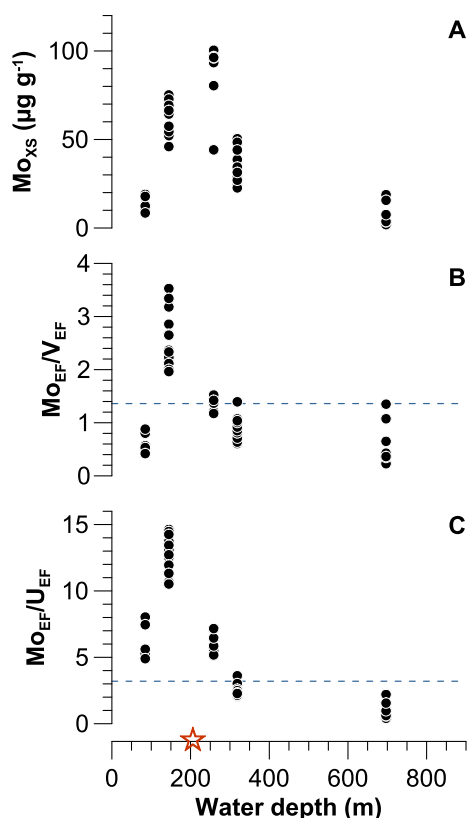


Fig. 5. Distribution of trace metals in shallow sediments: (A) Mo_{XS} , (B) $\text{Mo}_{\text{EF}}/\text{V}_{\text{EF}}$, (C) $\text{Mo}_{\text{EF}}/\text{U}_{\text{EF}}$. Horizontal dashed lines depict the dissolved Mo/V and Mo/U of seawater. The star above the x-axis depicts the water depth of M77-2-024-5. The data shown in this figure are contained in [Supplementary Table S2](#).

4.3. Solid phase and pore water molybdenum profiles in shallow sediments

The downcore distribution of pore water Mo, Mo_{XS} and $\delta^{98}\text{Mo}_{\text{XS}}$ is compared to the distribution of dissolved Fe and H_2S as well as solid phase Fe speciation for selected cores (Fig. 6, Table 1). The cores shown in Fig. 6 were chosen because they cover the transition from Fe-rich (ferruginous) to sulfidic pore water (the two other cores listed in Table 1 and plotted in Fig. 5 are shorter).

All three cores display elevated dissolved Mo concentrations in the topmost pore water sample compared to seawater and bottom water. This pore water concentration pattern indicates a flux of Mo from the sediment into the bottom water. In the shallower two cores with nitrogenous bottom water (145 m and 319 m water depth), the increase in pore water Mo coincides with increasing concentrations of dissolved Fe (Fig. 6A and B). Below a maximum at or close to the sediment surface, pore water Mo concentrations decrease and the lowest concentrations are observed at the depth where H_2S accumulates in the pore water. Higher dissolved Mo concentrations persist to greater sediment depth than dissolved Fe concentrations. The transition from Mo-enriched and ferruginous pore water to Mo-depleted and sulfidic pore water is accompanied by decreasing Fe (oxyhydr)oxide and increasing pyrite concentrations (Fig. 6A and B). The sediments are characterized by significant Mo enrichments throughout the cored depth interval ($\text{Mo}_{\text{XS}} > 20 \mu\text{g g}^{-1}$) and $\delta^{98}\text{Mo}_{\text{XS}}$ values fall into a relatively narrow range between $+1.25\text{‰}$ and $+1.52\text{‰}$.

At the deepest site (697 m water depth), where weakly oxic bottom waters prevail both dissolved ($\text{Mo} < 1100$ nM) and solid phase ($\text{Mo}_{\text{XS}} < 20 \mu\text{g g}^{-1}$) Mo concentrations increase towards the base of the core, coincident with decreasing Fe (oxyhydr)oxide and increasing pyrite concentrations (Fig. 6C). No H_2S was detected in this core. The $\delta^{98}\text{Mo}_{\text{XS}}$ consistently decrease from $+1.55\text{‰}$ at the sediment surface to $+1.04\text{‰}$ at the lower end of the core.

4.4. Paleo-record

The trace metal and Mo isotope variability in core M77-2-024-5 is compared with previously published nitrogen isotope data for the same record (Fig. 7). Reduction of nitrate to nitrite in the water column coupled to reduction of nitrite to N_2 by denitrification and anammox leaves the remaining nitrate enriched in ^{15}N . If the enriched nitrate is incorporated into phytoplankton biomass and subsequently preserved in the sediments a paleoceanographic record is created (Altabet et al., 2002). High $\delta^{15}\text{N}$ signatures during the late Holocene, the last deglaciation (BA) and the Eemian (Marine MIS5e), thus indicate more intense water column denitrification and anammox. In contrast, lower $\delta^{15}\text{N}$ values during MIS2 (last glacial), MIS3 and MIS5a through MIS5d indicate less intense denitrification and anammox (Fig. 7A). The temporal variability of Mo_{XS} is largely synchronous with the $\delta^{15}\text{N}$ record, i.e., higher Mo_{XS} is observed during the Holocene, MIS3 and MIS5e (Mo_{XS} up to $88 \mu\text{g g}^{-1}$) whereas lower Mo_{XS} is observed during MIS2, MIS4 and MIS5a though MIS5d (Mo_{XS} as low as

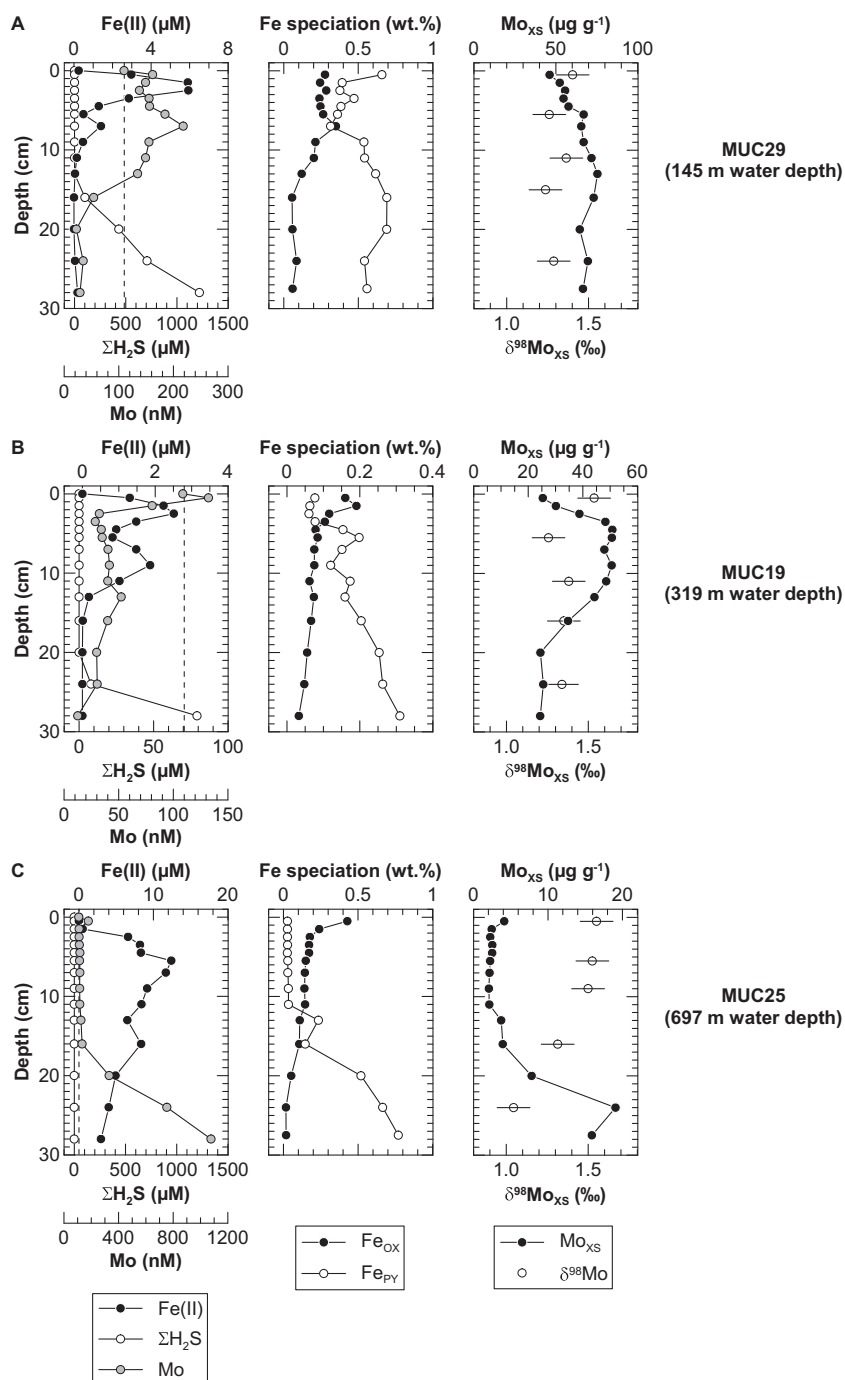


Fig. 6. Downcore profiles for (A) shelf sediments with predominantly nitrogenous bottom water, (B) slope sediments with nitrogenous bottom water, (C) slope sediments with weakly oxic bottom water: (left column) dissolved Fe, hydrogen sulfide and Mo in pore water (vertical dashed lines indicate seawater Mo concentration) (data from Scholz et al. (2011)); (central column) Fe (oxyhydr)oxide minerals (Fe_{ox}) leached with sodium dithionite and pyrite Fe (Fe_{py}) leached with HNO₃ after removal of the remaining Fe phases with HCl and HF (data from Scholz et al. (2014c), see there for methodological details); (right column) Mo_{XS} and δ⁹⁸Mo_{XS}. Note the different scales of the x-axes in (A), (B) and (C). The data shown in this figure are contained in the [Supplementary Tables S2 and S3](#).

6 μg g⁻¹) (Fig. 7B). The δ⁹⁸Mo_{XS} values range from +1.07‰ to +1.95‰ and do not significantly correlate with Mo_{XS} (Fig. 7C). The records of Mo_{EF}/V_{EF} and Mo_{EF}/U_{EF} display systematic variations that are synchronous with

Mo_{XS}. The higher Mo_{EF}/V_{EF} and Mo_{EF}/U_{EF} values are also consistent with the composition of particulate matter from the nitrogenous water column and surface sediments at the same water depth.

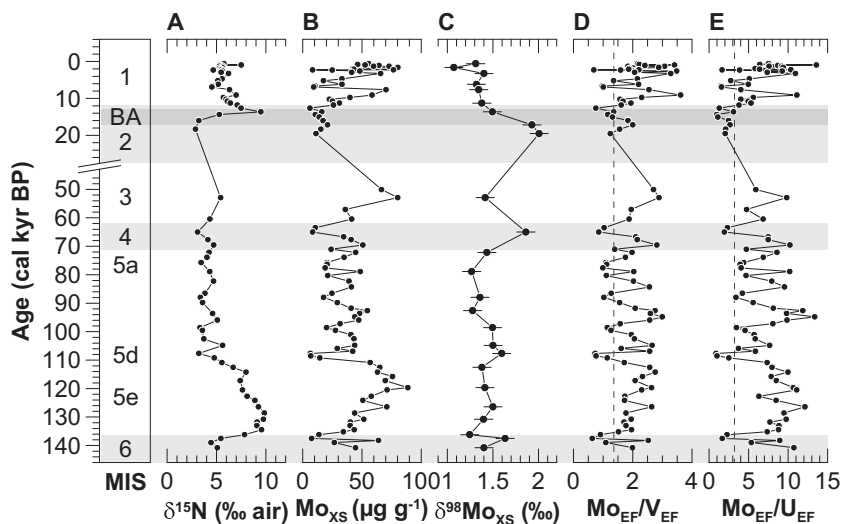


Fig. 7. Paleo-records of (A) $\delta^{15}\text{N}$, (B) Mo_{XS} , (C) $\delta^{98}\text{Mo}_{\text{XS}}$, (D) $\text{Mo}_{\text{EF}}/\text{V}_{\text{EF}}$, (E) $\text{Mo}_{\text{EF}}/\text{U}_{\text{EF}}$ (MIS: Marine Isotope Stage; BA: Bølling-Ållerød). Vertical dashed lines in (D) and (E) depict the dissolved Mo/V and Mo/U of seawater. The data shown in this figure are contained in Supplementary Table S4.

5. DISCUSSION

Sedimentary Mo_{XS} concentrations on the Peruvian shelf and through much of the paleo-record (Figs. 5A and 6B) by far exceed the threshold value for euxinic conditions of $25 \mu\text{g g}^{-1}$ (Scott and Lyons, 2012; Dahl et al., 2013b). Dissolved nitrogen species in the water column (Fig. 2B and C) as well as the nitrogen isotope record (Fig. 7A) indicate nitrogenous conditions at the same time. In general, H_2S does not accumulate in the water column unless nitrate and nitrite are quantitatively consumed, thus implying low or negligible enrichment of organic nitrogen in ^{15}N due to denitrification and anammox. Therefore, the presence of nitrate/nitrite in the water column along with the nitrogen isotope record presents a situation that is clearly inconsistent with euxinic conditions.

The Mo isotope data in the paleo-record presented here cover a $\delta^{98}\text{Mo}_{\text{XS}}$ range of almost 1‰ with the heaviest values being close to the Mo isotope composition of contemporary seawater. Surprisingly, the highest $\delta^{98}\text{Mo}_{\text{XS}}$ values are observed during intervals with low Mo_{XS} and $\delta^{15}\text{N}$ (MIS2 and MIS4), i.e., during intervals with presumably less reducing conditions.

These observations raise key-questions for the use and interpretation of Mo concentrations and Mo isotopes as paleo-redox proxies in open ocean settings, which will be discussed in detail below:

- (1) What is the mechanism of intense Mo delivery and accumulation at the Peruvian continental margin?
- (2) How do Mo isotopes in the sediment respond to this mechanism?
- (3) How relevant are the underlying processes for the interpretation of Mo concentrations and isotope ratios in the paleo-record?

5.1. Diffusive versus particulate molybdenum delivery

Previous studies have argued that Mo accumulation in sediments of productive upwelling regions is mediated through diffusion of Mo from the bottom water into the sulfidic zone of the sediment (Böning et al., 2004; Brumsack, 2006). The pore water profiles discussed in this study reveal an upward concentration gradient across the sediment-water interface (Fig. 6, left column), which is inconsistent with sedimentary Mo accumulation through diffusion. However, pore water profiles underlie a strong temporal variability and can only provide snapshot evidence for the mechanisms driving Mo accumulation. Therefore, a more general evaluation of diffusion-driven Mo mass accumulation rates is required to assess whether diffusion from bottom waters can explain the high Mo concentrations observed in Peru margin sediments.

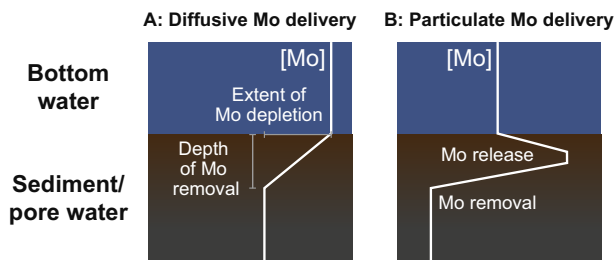


Fig. 8. Generalized representation of pore water Mo profiles being consistent with different mechanisms of Mo accumulation: (A) Accumulation through diffusion from the bottom water to the depth of Mo removal (extent of Mo depletion refers to the concentration difference between bottom water and the depth of Mo removal); (B) Mo release from a solid carrier phase followed by upward diffusion across the sediment water interface and downward diffusion to the depth of Mo removal. The solid phase Mo mass accumulation rate in (B) is higher because of the steeper concentration-depth gradient above the depth of Mo removal.

According to Fick's First Law, the accumulation rate of an element (Mo in the present case) through molecular diffusion at steady state depends on the ratio between the extent of element depletion and the depth over which element removal takes place (Fig. 8A). In addition, sediment diffusion is also affected by porosity and ambient temperature via the diffusion coefficient. We calculated diffusive fluxes of Mo into the sediment (hence Mo mass accumulation rates) for three end member scenarios of porosity and ambient temperature (Fig. 9). The three scenarios cover the full range of porosities and temperatures that may have prevailed at the coring location of M77-2-024-5 over the time span covered by the paleo-record. If Mo accumulated through diffusion, the time-integrated Mo mass accumulation rate would have to be consistent with the concentration-depth gradients implied by these scenarios.

The actual Mo_{XS} mass accumulation rates during the late Holocene, last glacial and Eemian were estimated by multiplying sedimentation rates, dry bulk densities and Mo_{XS} during the corresponding intervals (Table 2). Plotting these mass accumulation rates as continuous lines in Fig. 9 reveals that the high Mo_{XS} concentrations in sediments of the late Holocene and Eemian require complete Mo-depletion at very shallow depth (<0.1–2 cm). Such a shallow Mo depletion is not only inconsistent with the pore water profiles presented here (Fig. 6) but, to our best knowledge, with any pore water Mo profile in organic matter-rich sediments published to date (e.g., Zheng et al., 2000; Morford et al., 2005; Scholz et al., 2013). We therefore conclude that diffusion alone is an unrealistic mechanism of Mo accumulation in these sediments. Instead, a particulate Mo source forming in the water column has to be invoked to explain the extremely high Mo_{XS} concentrations in Peru margin sediments.

5.2. Molybdenum cycling in the water column

Considering the repeated detection of H_2S plumes during recent research cruises to the Peruvian margin

(Schunck et al., 2013; Sommer et al., 2016), it could be argued that interactions between Mo and H_2S in the water column are responsible for high Mo concentrations in shelf sediments (e.g., Dahl et al., 2013b). According to the traditional model, Mo removal from sulfidic waters requires the conversion of molybdate to thiomolybdate, which is possible at an aqueous H_2S ($\neq \Sigma\text{H}_2\text{S}$) concentration of $\geq 11 \mu\text{M}$ (Erickson and Helz, 2000). In a more recent study, Helz et al. (2011) pointed out that Mo might be removed from sulfidic waters as a nanoparticulate Fe-Mo-S mineral, which requires oversaturation with respect to amorphous Fe monosulfide. Concentrations of $\Sigma\text{H}_2\text{S}$ in recently sampled sulfidic plumes overlying the Peruvian shelf did not exceed $15 \mu\text{M}$ (Schunck et al., 2013; Scholz et al., 2016) and, considering the typical pH range of seawater, the majority of this H_2S was likely present as HS^- . Moreover, these weakly sulfidic waters were highly undersaturated with respect to Fe monosulfide (Scholz et al., 2016). From a thermodynamic point of view, water column Mo scavenging as aqueous Mo-S species or Fe-Mo-S nanoparticle is unlikely to take place under these conditions. Consistent with this notion, suspended particulate matter in sulfidic samples is least enriched in Mo compared to oxic and nitrogenous samples (Fig. 4B).

As an alternative to scavenging as Mo-S species or nanoparticulate Fe-Mo-S, Mo may be delivered to the sediment surface in association with Mn and Fe (oxyhydr)oxide minerals. Such a Mn and Fe shuttle mechanism has been postulated in an earlier study (Scholz et al., 2011) based on Mo-U covariation in the sediments (Algeo and Tribouillard, 2009). To evaluate the viability and elucidate the detailed mechanism of this supply pathway, we compare the distribution of particulate Mo with the distribution of other trace metals that are known to have some affinity for adsorption to metal (oxyhydr)oxides (i.e., V and U) (e.g., Chan and Riley, 1966; Wehrli and Stumm, 1989; Waite et al., 1994; Wang et al., 2012) as well as the distribution of particulate Mn and Fe carrier phases. All investigated trace metals show particulate enrichments in oxic

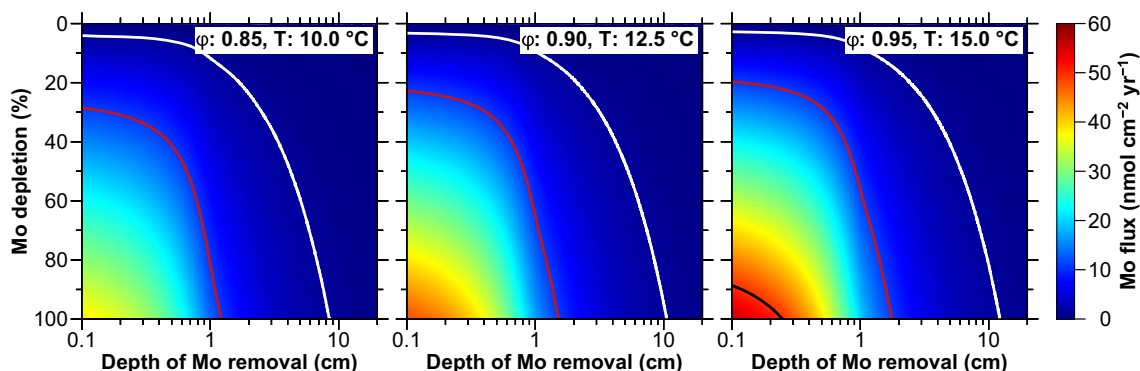


Fig. 9. Interpolated Mo mass accumulation rates calculated according to Fick's 1st Law as a function of the extent of Mo depletion (y-axis; 0% equals 110 nM) and the depth of Mo removal (x-axis; note log scale). The three panels represent three different scenarios of porosity and ambient temperature covering the range of values that may have prevailed in shelf sediments off Peru during the time span covered by the samples presented in this article. See Scholz et al. (2011) for details on the calculation. Solid lines depict the Mo mass accumulation rates observed during the late Holocene (black, only visible in the scenario with the highest temperature and porosity) last glacial (white) and the penultimate interglacial (red) (see also Table 2). (For interpretation of the references to colour in this figure legend, the reader is referred to the web version of this article.)

Table 2
Mo mass accumulation rates (MAR) during different time intervals in M77-2-024-5.

Time interval	Depth interval (cm)	Sedimentation rate ^a (cm yr ⁻¹)	Dry bulk density ^b (g cm ⁻³)	Mass accumulation rate (MAR) (g cm ⁻² yr ⁻¹)	Moxs (μg g ⁻¹)	SD (μg g ⁻¹)	Moxs-MAR (nmol cm ⁻² yr ⁻¹)	SD (nmol cm ⁻² yr ⁻¹)
Late Holocene	0–200	0.0679	1.35	9.17E-02	52.2	19.3	49.9	18.44
Last glacial	400–420	0.0085	1.35	1.15E-02	13.2	2.9	1.6	0.34
Eemian (MIS5e)	1100–1400	0.0138	1.35	1.86E-02	57.3	16.3	11.1	3.17

^a Mean sedimentation rate during the interval from Scholz et al. (2014b).

^b Dry bulk density of sediments from the same time interval at ODP Site 680 which is located at a similar water depth and in close vicinity to M77-2-024-5 (Shipboard Scientific Party, 1988).

surface waters (Fig. 4A–C), coincident with a pronounced maximum in particulate Mn/Al (Fig. 4F). This observation indicates that Mo is scavenged by Mn (oxyhydr)oxides in the surface ocean. Adsorption of Mo to organic matter (Wasylenki et al., 2007) could also be important in the productive surface waters of the Peruvian upwelling.

Manganese to Al ratios drop abruptly below the oxycline and, in contrast to Mo, particles within the nitrogenous zone are depleted in Mn relative to the regional lithogenic background. A similar trend of Mn depletion has been observed in other water column studies on the Peruvian margin (Hawco et al., 2016) and surface sediments are also strongly depleted in Mn relative to the lithogenic background (Böning et al., 2004; Scholz et al., 2011). According to these previous studies, most of the particulate Mn (oxyhydr)oxides present at the sea surface are reductively dissolved during sinking through the oxygen-depleted water mass. Consequently, any trace metals scavenged in the surface ocean by Mn (oxyhydr)oxides will not reach the sediment surface and particulate trace metal enrichments in the nitrogenous zone must be associated with another carrier phase.

Nitrogenous samples are characterized by elevated Fe/Al compared to both most of the oxic samples and the lithogenic background. Recently published X-ray absorption spectroscopy and other geochemical as well as metagenomic data for the same sample material suggest that these particulate Fe enrichments are formed through re-oxidation of sediment-derived dissolved Fe²⁺ with nitrate as terminal electron acceptor (Scholz et al., 2016). Nitrate-dependent Fe oxidation is relatively inefficient in demobilizing dissolved Fe compared to Fe oxidation in well-oxygenated surface sediments and bottom waters. Therefore, pore water Fe²⁺ can escape the sediment and be oxidized in the water column. We suggest that Fe is continually cycled between the sediments and overlying water through oxidation, deposition and dissolution until a fraction of it is retained and buried in the sediment. Repeated precipitation of Fe-rich particles in the water column by nitrate-dependent Fe oxidation and re-dissolution in the sediment provides an efficient transport mechanism for particle-reactive trace metals to the sediment surface. In agreement with this hypothesis, surface sediments in the nitrogenous OMZ display Mo_{EF}/V_{EF} and Mo_{EF}/U_{EF} similar to the particulate matter in the overlying water column (Fig. 5).

Further support for Mo deposition with Fe (oxyhydr)oxides is provided by the Mo isotope composition of the surface sediments. The average δ⁹⁸Mo_{XS} ± 1 SD observed in shallow sediment cores is +1.35 ± 0.13‰, which is in good agreement with the experimentally derived isotope composition of seawater Mo adsorbed to the Fe (oxyhydr)oxide minerals ferrihydrite (δ⁹⁸Mo = +1.2 ± 0.15) and goethite (δ⁹⁸Mo = +0.9 ± 0.48) (at pH 7.7; a smaller isotopic offset from seawater is to be expected at lower pH) (Goldberg et al., 2009). Both minerals have been shown to be abundant in the particulate matter in the nitrogenous zone of the Peruvian OMZ (Scholz et al., 2016). Other minerals that could play an important role in delivering Mo to the sediment surface in the nitrogenous

OMZ are mixed ferrous-ferric Fe minerals such as green rust (Heller et al., 2017). This type of mineral is known to form by anoxic Fe oxidation (Kappler and Newman, 2004; Pantke et al., 2012) and has a high adsorption capacity for particle-reactive trace metals (Zegeye et al., 2012). However, the isotopic effect associated with Mo adsorption to green rust has yet to be determined.

5.3. Early diagenesis of molybdenum

Pore water profiles of both dissolved Fe and Mo for the two shallow sediment cores from the nitrogenous OMZ display an increase from the bottom water into the surface sediment (Fig. 6a and b, left column). This observation is consistent with the scenario outlined in Fig. 8B, that is, Mo liberation upon reductive dissolution of Fe (oxyhydr)oxide minerals driving an upward-directed diffusive Fe and Mo flux across the sediment-bottom water interface. Below the dissolved Fe and Mo maxima, pore water Fe and Mo profiles are decoupled with near-complete Mo depletion occurring at greater sediment depth than Fe depletion. Fe removal is controlled by H₂S production through bacterial sulfate reduction. Since any H₂S produced immediately reacts with dissolved Fe in pore water and reactive Fe (oxyhydr)oxide minerals, H₂S does not accumulate in the pore water until the highly reactive Fe has been completely converted to sulfide minerals (Canfield et al., 1992). Efficient Mo removal from pore water as Mo-S-species requires the accumulation of H₂S in the pore water (Helz et al., 1996). Therefore, near-quantitative Mo scavenging from pore water occurs at greater sediment depth than Fe removal. However, even in the uppermost cm of the sediment, where no H₂S was detectable, Mo_{XS} concentrations range from 20 to 50 μg g⁻¹ (Fig. 6A and B, right column). Mo accumulation at this shallow depth could be related to co-precipitation with Fe monosulfide minerals or pyrite (Zheng et al., 2000), which are both present at this depth (Fig. 6A, central column and Fig. 2C and D in Scholz et al., 2014c), or to precipitation as nanoparticulate Fe-Mo-S (Helz et al., 2011). The importance of pyrite as a host phase for Mo in Peru margin sediments is highlighted by the coincident

increase of Mo_{XS} and pyrite concentrations despite the absence of dissolved H₂S in sediments below the OMZ (Fig. 6C).

All surface sediment samples display a negative correlation between δ⁹⁸Mo_{XS} and Mo_{XS} concentration (Fig. 6, right column, Fig. 10A). Part of this shift towards lighter Mo isotope compositions with depth and increasing Mo content may be related to the isotope fractionation associated with the conversion of molybdate to thiomolybdate species (Tossell, 2005) at the transition from ferruginous to sulfidic conditions in pore water. Alternatively or in addition, the isotopic shift may be related to the progressive scavenging of isotopically light dissolved Mo in pore water originating from the dissolution of Fe (oxyhydr)oxide minerals (the light Mo isotope composition was originally acquired during adsorption in the water column).

Sediments associated with nitrogenous bottom waters (Fig. 6A and B) and sediments with weakly oxic bottom waters (Fig. 6C) plot on separate correlation trends, with the latter being characterized by lighter δ⁹⁸Mo_{XS} at lower Mo_{XS} concentrations (Fig. 10A). Given that sediments and pore waters from all sites are uniformly depleted in Mn (Scholz et al., 2011), Mo delivery with Mn (oxyhydr)oxides is an unlikely explanation for the light Mo isotope composition of sediments at the site with weakly oxic bottom water. However, these sediments at the lower boundary of the OMZ are characterized by a higher content of crystalline Fe (oxyhydr)oxides (i.e., goethite and hematite) (Scholz et al., 2014c) and a higher concentration of Fe (oxyhydr)oxide minerals in general (Fig. 6C, central column). As Mo adsorbed to crystalline Fe (oxyhydr)oxides has a relatively light isotope composition (Goldberg et al., 2009), the differing slope of the correlation trends in Fig. 10A could be assigned to the difference in concentration and mineralogy of Fe (oxyhydr)oxide minerals.

To evaluate the fate of Mo and reactive Fe upon transition from ferruginous to sulfidic conditions during early diagenesis, we examine the Mo isotope composition as a function of the extent to which reactive Fe has been converted to pyrite (extent of pyritization, Fe_{PY}/(Fe_{OX} + Fe_{PY})) (Fig. 11A). In this diagram, the separate correlation trends between sediments with nitrogenous}

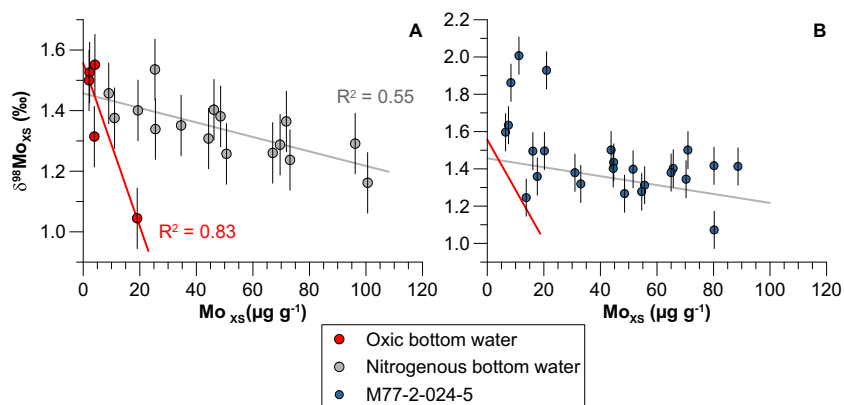


Fig. 10. Plot of δ⁹⁸Mo_{XS} versus Mo_{XS} for (A) shallow sediment core samples and (B) samples from the paleo-record (M77-2-024-5). The correlation trends displayed by sediments with nitrogenous and oxic bottom waters in (A) are also plotted in (B) for comparison.

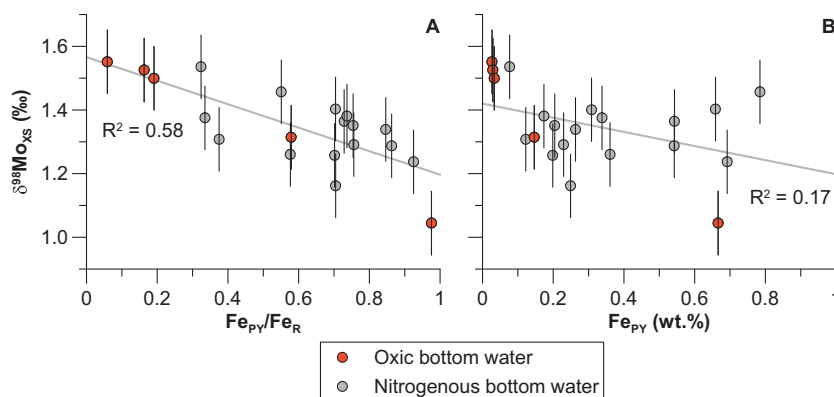


Fig. 11. Plot of (A) $\delta^{98}\text{Mo}_{\text{XS}}$ versus the extent to which Fe (oxyhydr)oxides have been converted to pyrite ($\text{Fe}_{\text{PY}}/(\text{Fe}_{\text{OX}} + \text{Fe}_{\text{PY}})$) and (B) $\delta^{98}\text{Mo}_{\text{XS}}$ versus pyrite concentration (Fe_{PY}) for shallow sediment core samples.

and oxic bottom water in Fig. 10A form one unique correlation. For comparison, no such correlation exists between $\delta^{98}\text{Mo}_{\text{XS}}$ and pyrite concentration (Fig. 11B). This observation indicates that not only the isotope composition of the Mo source (different Fe (oxyhydr)oxide minerals) and sink (presumably pyrite) phases but also the actual process of pyrite formation is important for the $\delta^{98}\text{Mo}_{\text{XS}}$ recorded in the geological record. Future work on the Mo isotope composition of sedimentary Fe pools combined with transport-reaction modeling may help to fully constrain the mechanisms driving Mo isotope fractionation during early sediment diagenesis.

5.4. Reconstruction of molybdenum cycling over the last 140,000 years

In the paleo-record, the highest Mo_{XS} concentrations coincide with high $\delta^{15}\text{N}$ values during the Eemian and late Holocene (Fig. 7A and B). Previous studies have demonstrated that these periods were (and still are in case of the late Holocene) characterized by strong oxygen-depletion in the bottom water and intense water column denitrification (Ganeshram et al., 2000; Scholz et al., 2014b; Salvatelli et al., 2015). Such conditions are conducive to sedimentary Fe release and re-precipitation of Fe (oxyhydr)oxide minerals in the nitrogenous water column through nitrate-dependent Fe oxidation (Scholz et al., 2014a, 2016). Taking into account our new findings on Mo cycling in the present-day water column and surface sediments, this nitrate-dependent Fe shuttle for Mo is likely responsible for the high Mo mass accumulation rates observed during the Eemian and late Holocene. This interpretation is supported by trace metal co-variation patterns revealing that the highest Mo_{XS} concentrations are accompanied by $\text{Mo}_{\text{EF}}/\text{V}_{\text{EF}}$ and $\text{Mo}_{\text{EF}}/\text{U}_{\text{EF}}$ higher than seawater (Fig. 7D and E) and are thus similar to those of suspended particulate matter and modern surface sediments in the nitrogenous OMZ (Figs. 4D, E and 5B, C).

Most of the $\delta^{98}\text{Mo}_{\text{XS}}$ signatures in core M77-2-024-5 are relatively uniform (Fig. 7C) and plot on the nitrogenous and weakly oxic correlation trends defined by modern surface sediments (compare Fig. 10A and B). A similar suite of processes, i.e., Mo delivery with variable Fe (oxyhydr)oxide

minerals, liberation into the pore water upon Fe reduction and re-precipitation with Fe sulfide minerals, has likely contributed to the Mo isotope composition of these sediments. However, there are a few samples with relatively high $\delta^{98}\text{Mo}_{\text{XS}}$ values ($\delta^{98}\text{Mo}_{\text{XS}}$ up to +1.95‰), which are isotopically heavier than any Mo isotope composition associated with metal oxides observed to date. Adsorption of seawater Mo is thus unlikely to be the reason for the sedimentary Mo isotope composition of these samples. All processes known to fractionate Mo isotopes in the marine environment produce lighter $\delta^{98}\text{Mo}$ values in the solid phase relative to the dissolved phase (Siebert et al., 2003; Barling and Anbar, 2004; Tossell, 2005; Wasylenki et al., 2008; Goldberg et al., 2009). Therefore, essentially unaltered seawater ($\delta^{98}\text{Mo} = +2.3‰$) is the only conceivable Mo source that can explain the relatively heavy $\delta^{98}\text{Mo}_{\text{XS}}$ values observed in certain intervals of M77-2-024-5.

Samples with the heaviest $\delta^{98}\text{Mo}_{\text{XS}}$ values correspond to sediments that were deposited during the glacial intervals MIS2 and MIS4 (Fig. 7C). These intervals are characterized by low $\delta^{15}\text{N}$ values, low Mo_{XS} as well as $\text{Mo}_{\text{EF}}/\text{V}_{\text{EF}}$ and $\text{Mo}_{\text{EF}}/\text{U}_{\text{EF}}$ lower than seawater (Fig. 7). This combination of proxy signals indicates less reducing conditions with little or no water column denitrification and, therefore, a lack of accelerated Mo delivery due to repeated dissolution of Fe (oxyhydr)oxide minerals in the sediment and nitrate-dependent re-oxidation of dissolved Fe in the water column. Samples with a high $\delta^{98}\text{Mo}_{\text{XS}}$ are characterized by low total Fe to Al (Fe_T/Al) ratios compared to the regional lithogenic background (Fig. 12), which is indicative of a diminished delivery or net retention of reactive Fe minerals (Raiswell and Canfield, 2012) on the Peruvian continental margin under glacial conditions (Scholz et al., 2014b). Under conditions where little reactive Fe is present in the sediments and, by inference, little Mo is released from Fe (oxyhydr)oxide minerals into the pore water, a direct concentration-depth gradient from the bottom water into the sediment can ensue. Such a scenario of diffusive Mo delivery (Fig. 8A) is generally consistent with the low Mo mass accumulation rates during glacial intervals, which can be explained with a reasonable depth of Mo depletion of 5–10 cm (Fig. 9) (see, e.g., Zheng et al. (2000) and Scholz et al. (2013) for comparable pore water profiles).

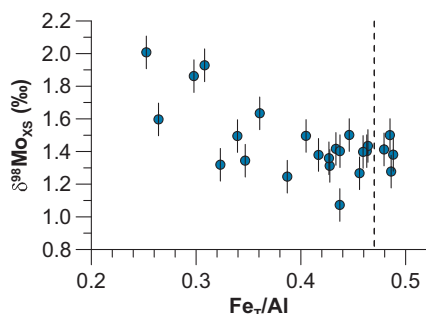


Fig. 12. Plot of $\delta^{98}\text{Mo}_{\text{XS}}$ versus Fe_T/Al for samples from the paleo-record (M77-2-024-5). The vertical dashed line depicts the Fe_T/Al of the regional lithogenic background.

Moreover, glacial sediments in core M77-2-024-5 display moderately high organic carbon (~ 0.9 wt.%) and total sulfur (~ 0.8 wt.%) concentrations (see [Supplementary Table S4](#)) indicating that hydrogen sulfide production was high enough to enable Mo fixation under sulfidic conditions at some depth below the sediment-water interface. In diffusion-dominated sedimentary systems, the expressed isotope fractionation factor decreases with the diffusive length-scale between the bottom water source and the depth of Mo fixation in the sediment ([Clark and Johnson, 2008](#)). Therefore, Mo fixation within the sediment coupled to a direct diffusive Mo flux from the bottom water is a viable explanation for the relatively heavy, seawater-like $\delta^{98}\text{Mo}_{\text{XS}}$ observed during glacial intervals.

6. SUMMARY AND IMPLICATIONS FOR THE USE OF MOLYBDENUM ISOTOPES AS A PALEO-REDOX PROXY

Sediments in the Peruvian OMZ are strongly enriched in Mo with interglacial Mo_{XS} concentrations being similar to those observed in restricted basins with sulfidic conditions in the water column. The water column of the Peruvian margin occasionally experiences sulfidic events. However, the water column particulate matter sampled in a sulfidic plume is depleted rather than enriched in Mo relative to oxic or anoxic-nitrogenous samples. Therefore, Mo scavenging under sulfidic conditions is ruled out as a major mechanism of Mo delivery to the sediment surface. Likewise, the mass accumulation rates observed during periods of peak Mo accumulation are too high as to be explained by diffusion of dissolved Mo from the bottom water into the sulfidic zone of the sediments.

Mn- and Fe-rich particles at the sea surface as well as Fe-rich particles in the OMZ are characterized by pronounced Mo enrichments. Mn (oxyhydr)oxides are efficiently dissolved during gravitational sinking through the anoxic water column. In contrast, Fe (oxyhydr)oxide-rich particles are preserved and the majority of Fe-rich particles form in the anoxic water column itself due to re-oxidation of sediment-derived dissolved Fe with nitrate as the terminal electron acceptor. Repeated recycling of reactive Fe between the sediment and the nitrogenous water column provides an efficient shuttle for particulate Mo to the sediment surface.

Some of the Mo that is released from Fe (oxyhydr)oxide minerals in the surface sediment is recycled into the bottom water by diffusion. The remaining Mo is co-precipitated with Fe sulfide minerals thus leading to high Mo burial rates. The Mo isotope composition of surface sediments and most samples from the paleo-record are consistent with Mo delivery adsorbed to Fe (oxyhydr)oxides and conversion to authigenic Mo-S phases during early diagenesis. A few samples from the paleo-record are characterized by exceptionally heavy isotope values close to the Mo isotope composition of modern seawater. Coeval proxy signals for reduced Mo delivery with Fe (oxyhydr)oxide minerals suggest that these heavy Mo isotope values can be explained by diffusion of bottom water Mo into a sulfidic reaction zone deeper in the sediment.

Our scenario of particulate Mo delivery and fixation in sulfidic sediments of the Peruvian OMZ is broadly consistent with the so-called particulate shuttle that has been proposed to explain high Mo mass accumulation rates in restricted euxinic basins with a short seawater residence time ([Algeo and Tribouillard, 2009](#)). These authors introduced sedimentary $\text{Mo}_{\text{EF}}/\text{U}_{\text{EF}}$ greater than seawater as the diagnostic proxy signal for this mode of Mo cycling. Peru margin sediments are characterized by similar $\text{Mo}_{\text{EF}}/\text{U}_{\text{EF}}$ as sediments from the euxinic Cariaco Basin and the Baltic Sea Deeps (see [Figs. 5C and 7E](#) as well as plots of Mo_{EF} versus U_{EF} in [Scholz et al. \(2011, 2013\)](#)). However, unlike implied by the original proxy rationale, the Peruvian continental margin is neither restricted nor euxinic and the generation of Fe- and Mo-rich particles is related to reductive processes in the nitrogen cycle rather than interactions with sulfide below or oxygen above the chemocline. We argue that a particulate shuttle for Mo is likely to operate in any anoxic marine environment with short seawater residence time, ranging from nitrogenous to euxinic. Importantly, as long as the reactive Fe present is repeatedly recycled between sediments and water column, accelerated delivery of Mo with Fe (oxyhydr)oxides does not require that the supply of reactive Fe is elevated overall (e.g., as indicated by elevated Fe_T/Al or highly reactive Fe over total Fe, $\text{Fe}_{\text{HR}}/\text{Fe}_T$) ([Fig. 12](#)).

Our findings demonstrate that a particulate shuttle for Mo generates a sedimentary Mo isotope value intermediate between seawater and riverine Mo input. Similar isotope values have been found in other anoxic, marine systems regardless if these are euxinic or not ([Fig. 1](#)) (e.g., [Arnold et al., 2004](#); [Poulson et al., 2006](#); [Poulson Brucker et al., 2009](#)). Any paleo-approach attempting to identify a globally reduced Mo inventory from a shift to lighter Mo isotope values in Black Shales needs to assess if particulate Mo delivery with Fe (or Mn) (oxyhydr)oxides can be ruled out. Otherwise, the Mo isotope fractionation associated with this shuttle needs to be taken into account in mass balance calculations.

ACKNOWLEDGEMENTS

We are grateful to the government of Peru for granting access to their territorial waters as well as to the crew of RV Meteor for supporting our research at sea. Thanks are due to A. Bleyer, A. Fis-

kal, B. Domeyer, E. Breitbarth, D. Nitschkowsky, R. Surberg and S. Steigenberger for technical and analytical assistance. Constructive comments by two anonymous reviewers and the associate editor Silke Severmann helped to improve the manuscript. This study was supported by the German Research Foundation through Sonderforschungsbereich 754 (“Climate-Biogeochemistry Interactions in the Tropical Ocean”) and the Emmy Noether Nachwuchsforschergruppe ICONOX (“Iron Cycling in Marine Sediments and the Oxygen and Nutrient Balance of the Ocean”) to FS.

APPENDIX A. SUPPLEMENTARY MATERIAL

Supplementary data associated with this article can be found, in the online version, at <http://dx.doi.org/10.1016/j.gca.2017.06.048>.

REFERENCES

- Algeo T. J. (2004) Can marine anoxic events draw down the trace element inventory of seawater? *Geology* **32**, 1057–1060.
- Algeo T. J. and Lyons T. W. (2006) Mo-total organic carbon covariation in modern anoxic marine environments: implications for analysis of paleoredox and paleohydrographic conditions. *Paleoceanography* **21**, PA1016.
- Algeo T. J. and Tribovillard N. (2009) Environmental analysis of paleoceanographic systems based on molybdenum-uranium covariation. *Chem. Geol.* **268**, 211–225.
- Altabet M. A., Higginson M. J. and Murray D. W. (2002) The effect of millennial-scale changes in Arabian Sea denitrification on atmospheric CO₂. *Nature* **415**, 159–162.
- Archer C. and Vance D. (2008) The isotopic signature of the global riverine molybdenum flux and anoxia in the ancient oceans. *Nat. Geosci.* **1**, 597–600.
- Arnold G. L., Anbar A. D., Barling J. and Lyons T. W. (2004) Molybdenum isotope evidence for widespread anoxia in mid-proterozoic oceans. *Science* **304**, 87–90.
- Barling J. and Anbar A. D. (2004) Molybdenum isotope fractionation during adsorption by manganese oxides. *Earth Planet. Sci. Lett.* **217**, 315–329.
- Barling J., Arnold G. L. and Anbar A. D. (2001) Natural mass-dependent variations in the isotopic composition of molybdenum. *Earth Planet. Sci. Lett.* **193**, 447–457.
- Bohlen L., Dale A. W., Sommer S., Mosch T., Hensen C., Noffke A., Scholz F. and Wallmann K. (2011) Benthic nitrogen cycling traversing the Peruvian oxygen minimum zone. *Geochim. Cosmochim. Acta* **75**, 6094–6111.
- Böning P., Brumsack H. J., Böttcher M. E., Schnetger B., Kriete C., Kallmeyer J. and Borchers S. L. (2004) Geochemistry of Peruvian near-surface sediments. *Geochim. Cosmochim. Acta* **68**, 4429–4451.
- Bruland K. W. (1983) Trace elements in seawater. In *Chemical Oceanography* (eds. J. P. Riley and R. Chester). Academic Press, New York, pp. 157–221.
- Bruland K. W., Rue E. L., Smith G. J. and DiTullio G. R. (2005) Iron, macronutrients and diatom blooms in the Peru upwelling regime: brown and blue waters of Peru. *Mar. Chem.* **93**, 81–103.
- Brumsack H.-J. (2006) The trace metal content of recent organic carbon-rich sediments: implications for Cretaceous black shale formation. *Palaeogeogr. Palaeoclimatol. Palaeoecol.* **232**, 344–361.
- Canfield D. E., Raiswell R. and Bottrell S. H. (1992) The reactivity of sedimentary iron minerals toward sulfide. *Am. J. Sci.* **292**, 659–683.
- Chan K. M. and Riley J. P. (1966) The determination of vanadium in sea and natural waters, biological materials and silicate sediments and rocks. *Anal. Chim. Acta* **34**, 337–345.
- Clark S. K. and Johnson T. M. (2008) Effective isotopic fractionation factors for solute removal by reactive sediments: a laboratory microcosm and slurry study. *Environ. Sci. Technol.* **42**, 7850–7855.
- Cutter, G., Andersson, P., Codispoti, L., Croot, P., Francois, R., Lohan, M., Obata, H., Rutgers van der Loeff, M., 2014. Sampling and Sample-handling Protocols for GEOTRACES Cruises. <www.geotraces.org/images/stories/documents/intercalibration/Cookbook.pdf>.
- Dahl T. W., Anbar A. D., Gordon G. W., Rosing M. T., Frei R. and Canfield D. E. (2010) The behavior of molybdenum and its isotopes across the chemocline and in the sediments of sulfidic Lake Cadagno, Switzerland. *Geochim. Cosmochim. Acta* **74**, 144–163.
- Dahl T. W., Canfield D. E., Rosing M. T., Frei R. E., Gordon G. W., Knoll A. H. and Anbar A. D. (2011) Molybdenum evidence for expansive sulfidic water masses in ~750 Ma oceans. *Earth Planet. Sci. Lett.* **311**, 264–274.
- Dahl T. W., Chappaz A., Fitts J. P. and Lyons T. W. (2013a) Molybdenum reduction in a sulfidic lake: Evidence from X-ray absorption fine-structure spectroscopy and implications for the Mo paleoproxy. *Geochim. Cosmochim. Acta* **103**, 213–231.
- Dahl T. W., Ruhl M., Hammarlund E. U., Canfield D. E., Rosing M. T. and Bjerrum C. J. (2013b) Tracing euxinia by molybdenum concentrations in sediments using handheld X-ray fluorescence spectroscopy (HHXRF). *Chem. Geol.* **360–361**, 241–251.
- Dale A. W., Sommer S., Lomnitz U., Bourbonnais A. and Wallmann K. (2016) Biological nitrate transport in sediments on the Peruvian margin mitigates benthic sulfide emissions and drives pelagic N loss during stagnation events. *Deep Sea Res. Part I* **112**, 123–136.
- Dalsgaard T., Thamdrup B., Fariás L. and Revsbech N. P. (2012) Anammox and denitrification in the oxygen minimum zone of the eastern South Pacific. *Limnol. Oceanogr.* **57**, 1331–1346.
- Emerson S. R. and Huested S. S. (1991) Ocean Anoxia and the concentrations of molybdenum and vanadium in seawater. *Mar. Chem.* **34**, 177–196.
- Erickson B. E. and Helz G. R. (2000) Molybdenum(VI) speciation in sulfidic waters: Stability and lability of thiomolybdates. *Geochim. Cosmochim. Acta* **64**, 1149–1158.
- Freyruth H., Vils F., Willbold M., Taylor R. N. and Elliott T. (2015) Molybdenum mobility and isotopic fractionation during subduction at the Mariana arc. *Earth Planet. Sci. Lett.* **432**, 176–186.
- Ganeshram R. S., Pedersen T. F., Calvert S. E., McNeill G. W. and Fontugne M. R. (2000) Glacial-interglacial variability in denitrification in the World’s Oceans: causes and consequences. *Paleoceanography* **15**, 361–376.
- Goldberg T., Archer C., Vance D. and Poulton S. W. (2009) Mo isotope fractionation during adsorption to Fe (oxyhydr)oxides. *Geochim. Cosmochim. Acta* **73**, 6502–6516.
- Goldberg T., Archer C., Vance D., Thamdrup B., McAnena A. and Poulton S. W. (2012) Controls on Mo isotope fractionations in a Mn-rich anoxic marine sediment, Gullmar Fjord, Sweden. *Chem. Geol.* **296–297**, 73–82.
- Goldberg T., Poulton S. W., Wagner T., Kolonic S. F. and Rehkämper M. (2016) Molybdenum drawdown during Cretaceous Oceanic Anoxic Event 2. *Earth Planet. Sci. Lett.* **440**, 81–91.
- Greber N. D., Siebert C., Nägler T. F. and Pettke T. (2012) $\Delta^{98/95}\text{Mo}$ values and Molybdenum Concentration Data for

- NIST SRM 610, 612 and 3134: towards a Common Protocol for Reporting Mo Data. *Geostand. Geoanal. Res.* **36**, 291–300.
- Gutiérrez D., Enríquez E., Purca S., Quipúzcoa L., Marquina R., Flores G. and Graco M. (2008) Oxygenation episodes on the continental shelf of central Peru: remote forcing and benthic ecosystem response. *Prog. Oceanogr.* **79**, 177–189.
- Hammarlund E. U., Dahl T. W., Harper D. A. T., Bond D. P. G., Nielsen A. T., Bjerrum C. J., Schovsbo N. H., Schönlaub H. P., Zalasiewicz J. A. and Canfield D. E. (2012) A sulfidic driver for the end-Ordovician mass extinction. *Earth Planet. Sci. Lett.* **331–332**, 128–139.
- Hawco N. J., Ohnemus D. C., Resing J. A., Twining B. S. and Saito M. A. (2016) A dissolved cobalt plume in the oxygen minimum zone of the eastern tropical South Pacific. *Biogeosciences* **13**, 5697–5717.
- Heller M. I., Lam P. J., Moffett J. W., Till C. P., Lee J.-M., Toner B. M. and Marcus M. A. (2017) Accumulation of Fe oxyhydroxides in the Peruvian oxygen deficient zone implies non-oxygen dependent Fe oxidation. *Geochim. Cosmochim. Acta* **211**, 174–193.
- Helz G. R., Miller C. V., Charnock J. M., Mosselmans J. F. W., Patrick R. A. D., Garner C. D. and Vaughan D. J. (1996) Mechanism of molybdenum removal from the sea and its concentration in black shales: EXAFS evidence. *Geochim. Cosmochim. Acta* **60**, 3631–3642.
- Helz G. R., Bura-Nakic E., Mikac N. and Ciglenecki I. (2011) New model for molybdenum behavior in euxinic waters. *Chem. Geol.* **284**, 323–332.
- Huerta-Diaz M. A. and Morse J. W. (1992) Pyritization of trace metals in anoxic marine sediments. *Geochim. Cosmochim. Acta* **56**, 2681–2702.
- Kappler A. and Newman D. K. (2004) Formation of Fe(III)-minerals by Fe(II)-oxidizing photoautotrophic bacteria. *Geochim. Cosmochim. Acta* **68**, 1217–1226.
- Kendall B., Creaser R. A., Gordon G. W. and Anbar A. D. (2009) Re-Os and Mo isotope systematics of black shales from the Middle Proterozoic Velkerri and Wollgorang Formations, McArthur Basin, northern Australia. *Geochim. Cosmochim. Acta* **73**, 2534–2558.
- Lam P., Lavik G., Jensen M. M., van de Vossenbergh J., Schmid M., Woebken D., Gutiérrez D., Amann R., Jetten M. S. M. and Kuypers M. M. M. (2009) Revising the nitrogen cycle in the Peruvian oxygen minimum zone. *Proc. Natl. Acad. Sci.* **106**, 4752–4757.
- Levin L., Gutiérrez D., Rathburn A., Neira C., Sellanes J., Muñoz P., Gallardo V. and Salamanca M. (2002) Benthic processes on the Peru margin: a transect across the oxygen minimum zone during the 1997–98 El Niño. *Prog. Oceanogr.* **53**, 1–27.
- Malinovsky D., Hammarlund D., Ilyashuk B., Martinsson O. and Gelting J. (2007) Variations in the isotopic composition of molybdenum in freshwater lake systems. *Chem. Geol.* **236**, 181–198.
- McManus J., Nägler T. F., Siebert C., Wheat C. G. and Hammond D. E. C. (2002) Oceanic molybdenum isotope fractionation: Diagenesis and hydrothermal ridge-flank alteration. *Geochem. Geophys. Geosyst.* **3**, 1–9.
- McManus J., Berelson W. M., Severmann S., Poulson R. L., Hammond D. E., Klinkhammer G. P. and Holm C. (2006) Molybdenum and uranium geochemistry in continental margin sediments: Paleoproxy potential. *Geochim. Cosmochim. Acta* **70**, 4643–4662.
- Miller C. A., Peucker-Ehrenbrink B., Walker B. D. and Marcantonio F. (2011) Re-assessing the surface cycling of molybdenum and rhenium. *Geochim. Cosmochim. Acta* **75**, 7146–7179.
- Morford J. L., Emerson S. R., Breckel E. J. and Kim S. H. (2005) Diagenesis of oxyanions (V, U, Re, and Mo) in pore waters and sediments from a continental margin. *Geochim. Cosmochim. Acta* **69**, 5021–5032.
- Muratli J. M., Chase Z., Mix A. C. and McManus J. (2010) Increased glacial-age ventilation of the Chilean margin by Antarctic Intermediate Water. *Nat. Geosci.* **3**, 23–26.
- Muratli J. M., McManus J., Mix A. and Chase Z. (2012) Dissolution of fluoride complexes following microwave-assisted hydrofluoric acid digestion of marine sediments. *Talanta* **89**, 195–200.
- Nägler T. F., Neubert N., Böttcher M. E., Dellwig O. and Schnetger B. (2011) Molybdenum isotope fractionation in pelagic euxinia: Evidence from the modern Black and Baltic Seas. *Chem. Geol.* **289**, 1–11.
- Nägler T. F., Anbar A. D., Archer C., Goldberg T., Gordon G. W., Greber N. D., Siebert C., Sohrin Y. and Vance D. (2014) Proposal for an International Molybdenum Isotope Measurement Standard and Data Representation. *Geostand. Geoanal. Res.* **38**, 149–151.
- Neubert N., Nägler T. F. and Böttcher M. E. (2008) Sulfidity controls molybdenum isotope fractionation into euxinic sediments: evidence from the modern Black Sea. *Geology* **36**, 775–778.
- Noffke A., Hensen C., Sommer S., Scholz F., Bohlen L., Mosch T., Graco M. and Wallmann K. (2012) Benthic iron and phosphorus fluxes across the Peruvian oxygen minimum zone. *Limnol. Oceanogr.* **57**, 851–867.
- Noordmann J., Weyer S., Montoya-Pino C., Dellwig O., Neubert N., Eckert S., Paetzel M. and Böttcher M. E. (2015) Uranium and molybdenum isotope systematics in modern euxinic basins: case studies from the central Baltic Sea and the Kyllaren fjord (Norway). *Chem. Geol.* **396**, 182–195.
- Pantke C., Obst M., Benzerara K., Morin G., Ona-Nguema G., Dippon U. and Kappler A. (2012) Green rust formation during Fe(II) oxidation by the nitrate-reducing *Acidovorax* sp. strain BoFeN1. *Environ. Sci. Technol.* **46**, 1439–1446.
- Poulson R. L., Siebert C., McManus J. and Berelson W. M. (2006) Authigenic molybdenum isotope signatures in marine sediments. *Geology* **34**, 617–620.
- Poulson Brucker R. L., McManus J., Severmann S. and Berelson W. M. (2009) Molybdenum behavior during early diagenesis: Insights from Mo isotopes. *Geochem. Geophys. Geosyst.* **10**.
- Poulton S. W., Fralick P. W. and Canfield D. E. (2010) Spatial variability in oceanic redox structure 1.8 billion years ago. *Nat. Geosci.* **3**, 486–490.
- Raiswell R. and Canfield D. E. (2012) The iron biogeochemical cycle past and present. *Geochem. Perspect.* **1**, 1–220.
- Richards F. A. (1965) Anoxic basins and fjords. In *Chemical Oceanography* (eds. J. P. Riley and G. Skirrow). Academic Press, New York, pp. 611–643.
- Salvatteci R., Gutierrez D., Sifeddine A., Ortlieb L., Druffel E., Boussafir M. and Schneider R. (2015) Centennial to millennial-scale changes in oxygenation and productivity in the Eastern Tropical South Pacific during the last 25,000 years. *Quatern. Sci. Rev.* **131**(Part A), 102–117.
- Scholz F., Hensen C., Noffke A., Rohde A., Liebetrau V. and Wallmann K. (2011) Early diagenesis of redox-sensitive trace metals in the Peru upwelling area: response to ENSO-related oxygen fluctuations in the water column. *Geochim. Cosmochim. Acta* **75**, 7257–7276.
- Scholz F., McManus J. and Sommer S. (2013) The manganese and iron shuttle in a modern euxinic basin and implications for molybdenum cycling at euxinic ocean margins. *Chem. Geol.* **355**, 56–68.
- Scholz F., Severmann S., McManus J. and Hensen C. (2014a) Beyond the Black Sea paradigm: the sedimentary fingerprint of

- an open-marine iron shuttle. *Geochim. Cosmochim. Acta* **127**, 368–380.
- Scholz F., McManus J., Mix A. C., Hensen C. and Schneider R. R. (2014b) The impact of ocean deoxygenation on iron release from continental margin sediments. *Nat. Geosci.* **7**, 433–437.
- Scholz F., Severmann S., McManus J., Noffke A., Lomnitz U. and Hensen C. (2014c) On the isotope composition of reactive iron in marine sediments: Redox shuttle versus early diagenesis. *Chem. Geol.* **389**, 48–59.
- Scholz F., Löscher C. R., Fiskal A., Sommer S., Hensen C., Lomnitz U., Wuttig K., Göttlicher J., Kossel E., Steininger R. and Canfield D. E. (2016) Nitrate-dependent iron oxidation limits iron transport in anoxic ocean regions. *Earth Planet. Sci. Lett.* **454**, 272–281.
- Schunck H., Lavik G., Desai D. K., Grosskopf T., Kalvelage T., Loescher C. R., Paulmier A., Contreras S., Siegel H., Holtappels M., Rosenstiel P., Schilhabel M. B., Graco M., Schmitz R. A., Kuypers M. M. M. and LaRoche J. (2013) Giant hydrogen sulfide plume in the oxygen minimum zone off Peru supports chemolithoautotrophy. *PLoS ONE* **8**.
- Scott C. and Lyons T. W. (2012) Contrasting molybdenum cycling and isotopic properties in euxinic versus non-euxinic sediments and sedimentary rocks: Refining the paleoproxies. *Chem. Geol.* **324–325**, 19–27.
- Siebert C., Nägler T. F. and Kramers J. D. C. (2001) Determination of molybdenum isotope fractionation by double-spike multicollector inductively coupled plasma mass spectrometry. *Geochem. Geophys. Geosyst.* **2**. <http://dx.doi.org/10.1029/2000GC000124>.
- Siebert C., Nägler T. F., von Blanckenburg F. and Kramers J. D. (2003) Molybdenum isotope records as a potential new proxy for paleoceanography. *Earth Planet. Sci. Lett.* **211**, 159–171.
- Sommer S., Gier J., Treude T., Lomnitz U., Dengler M., Cardich J. and Dale A. W. (2016) Depletion of oxygen, nitrate and nitrite in the Peruvian oxygen minimum zone cause an imbalance of benthic nitrogen fluxes. *Deep Sea Res. Part I* **112**, 113–122.
- Thamdrup B., Dalsgaard T. and Revsbech N. P. (2012) Widespread functional anoxia in the oxygen minimum zone of the Eastern South Pacific. *Deep Sea Res. Part I* **65**, 36–45.
- Tossell J. A. (2005) Calculating the partitioning of the isotopes of Mo between oxidic and sulfidic species in aqueous solution. *Geochim. Cosmochim. Acta* **69**, 2981–2993.
- Tribouillard N., Riboulleau A., Lyons T. and Baudin F. (2004) Enhanced trapping of molybdenum by sulfurized marine organic matter of marine origin in Mesozoic limestones and shales. *Chem. Geol.* **213**, 385–401.
- Tribouillard N., Algeo T. J., Lyons T. W. and Riboulleau A. (2006) Trace metals as paleoredox and paleoproductivity proxies: An update. *Chem. Geol.* **232**, 12–32.
- Vedamati J., Goepfert T. and Moffett J. W. (2014) Iron speciation in the eastern tropical South Pacific oxygen minimum zone off Peru. *Limnol. Oceanogr.* **59**, 1945–1957.
- Voegelin A. R., Pettke T., Greber N. D., von Niederhäusern B. and Nägler T. F. (2014) Magma differentiation fractionates Mo isotope ratios: Evidence from the Kos Plateau Tuff (Aegean Arc). *Lithos* **190–191**, 440–448.
- Vorliceck T. P. and Helz G. R. (2002) Catalysis by mineral surfaces: Implications for Mo geochemistry in anoxic environments. *Geochim. Cosmochim. Acta* **66**, 3679–3692.
- Vorliceck T. P., Kahn M. D., Kasuya Y. and Helz G. R. (2004) Capture of molybdenum in pyrite-forming sediments: Role of ligand-induced reduction by polysulfides. *Geochim. Cosmochim. Acta* **68**, 547–556.
- Waite T. D., Davis J. A., Payne T. E., Waychunas G. A. and Xu N. (1994) Uranium(VI) adsorption to ferrihydrite: application of a surface complexation model. *Geochim. Cosmochim. Acta* **58**, 5465–5478.
- Wang Z., Lee S.-W., Catalano J. G., Lezama-Pacheco J. S., Bargar J. R., Tebo B. M. and Giammar D. E. (2012) Adsorption of uranium(VI) to manganese oxides: X-ray absorption spectroscopy and surface complexation modeling. *Environ. Sci. Technol.* **47**, 850–858.
- Wasylenki L. E., Anbar A. D., Liermann L. J., Mathur R., Gordon G. W. and Brantley S. L. (2007) Isotope fractionation during microbial metal uptake measured by MC-ICP-MS. *J. Anal. At. Spectrom.* **22**, 905–910.
- Wasylenki L. E., Rolfe B. A., Weeks C. L., Spiro T. G. and Anbar A. D. (2008) Experimental investigation of the effects of temperature and ionic strength on Mo isotope fractionation during adsorption to manganese oxides. *Geochim. Cosmochim. Acta* **72**, 5997–6005.
- Wehrli B. and Stumm W. (1989) Vanadyl in natural waters: adsorption and hydrolysis promote oxygenation. *Geochim. Cosmochim. Acta* **53**, 69–77.
- Westermann S., Vance D., Cameron V., Archer C. and Robinson S. A. (2014) Heterogeneous oxygenation states in the Atlantic and Tethys oceans during Oceanic Anoxic Event 2. *Earth Planet. Sci. Lett.* **404**, 178–189.
- Wille M., Nägler T. F., Lehmann B., Schroder S. and Kramers J. D. (2008) Hydrogen sulphide release to surface waters at the Precambrian/Cambrian boundary. *Nature* **453**, 767–769.
- Zegeye A., Bonneville S., Benning L. G., Sturm A., Fowle D. A., Jones C., Canfield D. E., Ruby C., MacLean L. C., Nomosatryo S., Crowe S. A. and Poulton S. W. (2012) Green rust formation controls nutrient availability in a ferruginous water column. *Geology* **40**, 599–602.
- Zheng Y., Anderson R. F., van Geen A. and Kuwabara J. (2000) Authigenic molybdenum formation in marine sediments: a link to pore water sulfide in the Santa Barbara Basin. *Geochim. Cosmochim. Acta* **64**, 4165–4178.

Associate Editor: Silke Severmann